Frames

A signal representation may provide "analysis" coefficients that are inner products with a family of vectors, or "synthesis" coefficients that compute an approximation by recombining a family of vectors. Frames are families of vectors where "analysis" and "synthesis" representations are stable. Signal reconstructions are computed with a dual frame. Frames are potentially redundant and thus more general than bases, with a redundancy measured by frame bounds. They provide the flexibility needed to build signal representations with unstructured families of vectors.

Complete and stable wavelet and windowed Fourier transforms are constructed with frames of wavelets and windowed Fourier atoms. In two dimensions, frames of directional wavelets and curvelets are introduced to analyze and process multiscale image structures.

5.1 FRAMES AND RIESZ BASES

5.1.1 Stable Analysis and Synthesis Operators

The frame theory was originally developed by Duffin and Schaeffer [235] to reconstruct band-limited signals from irregularly spaced samples. They established general conditions to recover a vector f in a Hilbert space $\mathbf{H}$ from its inner products with a family of vectors $\{\phi_n\}_{n\in\Gamma}$. The index set Γ might be finite or infinite. The following frame definition gives an energy equivalence to invert the operator Φ defined by

$$\forall n \in \Gamma, \quad \Phi f[n] = \langle f, \phi_n \rangle. \tag{5.1}$$

Definition 5.1: *Frame and Riesz Basis.* The sequence $\{\phi_n\}_{n\in\Gamma}$ is a frame of $\mathbf{H}$ if there exist two constants $B \geqslant A > 0$ such that

$$\forall f \in \mathbf{H}, \quad A \|f\|^2 \leqslant \sum_{n\in\Gamma} |\langle f, \phi_n \rangle|^2 \leqslant B \|f\|^2. \tag{5.2}$$

When $A = B$ the frame is said to be tight. If the $\{\phi_n\}_{n\in\Gamma}$ are linearly independant then the frame is not redundant and is called a *Riesz basis*.

If the frame condition is satisfied, then Φ is called a *frame analysis operator*. Section 5.1.2 proves that (5.2) is a necessary and sufficient condition guaranteeing that Φ is invertible on its image space, with a bounded inverse. Thus, a frame defines a complete and stable signal representation, which may also be redundant.

Frame Synthesis

Let us consider the space of finite energy coefficients

$$\ell^2(\Gamma) = \{a \,:\, \|a\|^2 = \sum_{n \in \Gamma} |a[n]|^2 < +\infty\}.$$

The adjoint Φ^* of Φ is defined over $\ell^2(\Gamma)$ and satisfies for any $f \in \mathbf{H}$ and $a \in \ell^2(\Gamma)$:

$$\langle \Phi^* a, f \rangle = \langle a, \Phi f \rangle = \sum_{n \in \Gamma} a[n] \langle f, \phi_n \rangle^*.$$

It is therefore the synthesis operator

$$\Phi^* a = \sum_{n \in \Gamma} a[n]\, \phi_n. \tag{5.3}$$

The frame condition (5.2) can be rewritten as

$$\forall f \in \mathbf{H}, \quad A\,\|f\|^2 \leq \|\Phi f\|^2 = \langle \Phi^* \Phi f, f \rangle \leq B\,\|f\|^2, \tag{5.4}$$

with

$$\Phi^* \Phi f = \sum_{m \in \Gamma} \langle f, \phi_n \rangle\, \phi_n.$$

It results that A and B are the infimum and supremum values of the spectrum of the symmetric operator $\Phi^* \Phi$, which correspond to the smallest and largest eigenvalues in finite dimension. The eigenvalues are also called *singular values* of Φ or *singular spectrum*. Theorem 5.1 derives that the frame synthesis operator is also stable.

Theorem 5.1. The family $\{\phi_n\}_{n \in \Gamma}$ is a frame with bounds $0 < A \leq B$ if and only if

$$\forall a \in \mathbf{Im}\Phi, \quad A\,\|a\|^2 \leq \|\sum_{n \in \Gamma} a[n]\,\phi_n\|^2 \leq B\,\|a\|^2. \tag{5.5}$$

Proof. Since $\Phi^* a = \sum_{n \in \Gamma} a[n]\, \phi_n$, it results that

$$\|\sum_{n \in \Gamma} a[n]\, \phi_n\|^2 = \langle \Phi\, \Phi^* a, a \rangle.$$

The operator Φ is a frame if and only if the spectrum of $\Phi^* \Phi$ is bound by A and B. The inequality (5.5) states that the spectrum of $\Phi\, \Phi^*$ over $\mathbf{Im}\Phi$ is also bounded by A and B. Both statements are proved to be equivalent by verifying that the supremum and infimum of the spectrum of $\Phi^* \Phi$ are equal to the supremum and infimum of the spectrum of $\Phi^* \Phi$.

In finite dimension, if λ is an eigenvalue of $\Phi^* \Phi$ with eigenvector f, then λ is also an eigenvalue of $\Phi^* \Phi$ with eigenvector Φf. Indeed, $\Phi^* \Phi f = \lambda f$ so $\Phi\, \Phi^*(\Phi f) = \lambda \Phi f$

and $\Phi f \neq 0$, because the left frame inequality (5.2) implies that $\|\Phi f\|^2 \leqslant A \|f\|^2$. It results that the maximum and minimum eigenvectors of $\Phi^* \Phi$ and $\Phi \Phi^*$ on $\mathbf{Im}\Phi$ are identical.

   In a Hilbert space of infinite dimension, we prove that the supremum and infimum of the spectrum of both operators remain identical by growing the space dimension, and computing the limit of the largest and smallest eigenvalues when the space dimension tends to infinity. ∎

This theorem proves that linear combination of frame vectors define a stable signal representation. Section 5.1.2 proves that synthesis coefficients are computed with a dual frame. The operator $\Phi \Phi^*$ is the *Gram* matrix $\{\langle \phi_n, \phi_p \rangle\}_{(m,p)\in\ell^2(\Gamma)}$:

$$\Phi \Phi^* a[p] = \sum_{m\in\Gamma} a[m] \langle \phi_n, \phi_p \rangle . \tag{5.6}$$

One must be careful because (5.5) is only valid for $a \in \mathbf{Im}\Phi$. If it is valid for all $a \in \ell^2(\Gamma)$ with $A > 0$ then the family is linearly independant and is thus a Riesz basis.

Redundancy
When the frame vectors are normalized $\|\phi_n\| = 1$, Theorem 5.2 shows that the frame redundancy is measured by the frame bounds A and B.

Theorem 5.2. In a space of finite dimension N, a frame of $P \geqslant N$ normalized vectors has frame bounds A and B, which satisfy

$$A \leqslant \frac{P}{N} \leqslant B. \tag{5.7}$$

For a tight frame $A = B = P/N$.

Proof. It results from (5.4) that all eigenvalues of $\Phi^* \Phi$ are between A and B. The trace of $\Phi^* \Phi$ thus satisfies

$$AN \leqslant \mathrm{tr}(\Phi^* \Phi) \leqslant BN.$$

But since the trace is not modified by commuting matrices (Exercise 5.4), and $\|\phi_n\| = 1$,

$$AN \leqslant \mathrm{tr}(\Phi^* \Phi) = \mathrm{tr}(\Phi \Phi^*) = \sum_{n=1}^{P} |\langle \phi_n, \phi_n \rangle|^2 = P \leqslant BN,$$

which implies (5.7). ∎

   If $\{\phi_n\}_{n\in\Gamma}$ is a normalized Riesz basis and is therefore linearly independent, then (5.7) proves that $A \leqslant 1 \leqslant B$. This result remains valid in infinite dimension. Inserting $f = \phi_n$ in the frame inequality (5.2) proves that the frame is orthonormal if and only if $B = 1$, in which case $A = 1$.

EXAMPLE 5.1

Let $\{g_1, g_2\}$ be an orthonormal basis of an $N = 2$ two-dimensional plane **H**. The $P = 3$ normalized vectors

$$\phi_1 = g_1, \quad \phi_2 = -\frac{g_1}{2} + \frac{\sqrt{3}}{2} g_2, \quad \phi_3 = -\frac{g_1}{2} - \frac{\sqrt{3}}{2} g_2$$

have equal angles of $2\pi/3$ between each other. For any $f \in \mathbf{H}$,

$$\sum_{n=1}^{3} |\langle f, \phi_n \rangle|^2 = \frac{3}{2} \|f\|^2.$$

Thus, these three vectors define a tight frame with $A = B = 3/2$.

EXAMPLE 5.2

For any $0 \leqslant k < K$, suppose that $\{\phi_{k,n}\}_{n \in \Gamma}$ is an orthonormal basis of **H**. The union of these K orthonormal bases $\{\phi_{k,n}\}_{n \in \Gamma, 0 \leqslant k < K}$ is a tight frame with $A = B = K$. Indeed, the energy conservation in an orthonormal basis implies that for any $f \in \mathbf{H}$,

$$\sum_{n \in \mathbb{Z}} |\langle f, \phi_{k,n} \rangle|^2 = \|f\|^2,$$

therefore,

$$\sum_{k=0}^{K-1} \sum_{n \in \mathbb{Z}} |\langle f, \phi_{k,n} \rangle|^2 = K \|f\|^2.$$

One can verify (Exercise 5.3) that a finite set of N vectors $\{\phi_n\}_{1 \leqslant n \leqslant N}$ is always a frame of the space **V** generated by linear combinations of these vectors. When N increases, the frame bounds A and B may go respectively to 0 and $+\infty$. This illustrates the fact that in infinite dimensional spaces, a family of vectors may be complete and not yield a stable signal representation.

Irregular Sampling

Let $\mathbf{U}_s$ be the space of $\mathbf{L}^2(\mathbb{R})$ functions having a Fourier transform support included in $[-\pi/s, \pi/s]$. For a uniform sampling, $t_n = ns$, Theorem 3.5 proves that if $\phi_s(t) = s^{1/2} \sin(\pi s^{-1} t)/(\pi t)$, then $\{\phi_s(t - ns)\}_{n \in \mathbb{Z}}$ is an orthonormal basis of $\mathbf{U}_s$. The reconstruction of f from its samples is then given by the sampling Theorem 3.2.

The irregular sampling conditions of Duffin and Schaeffer [235] for constructing a frame were later refined by several researchers [81, 102, 500]. Gröchenig proved [285] that if $\lim_{n \to +\infty} t_n = +\infty$ and $\lim_{n \to -\infty} t_n = -\infty$, and if the maximum sampling distance δ satisfies

$$\delta = \sup_{n \in \mathbb{Z}} |t_{n+1} - t_n| < s, \tag{5.8}$$

then

$$\{\lambda_n \, \phi_s(t - t_n)\}_{n \in \mathbb{Z}} \quad \text{with} \quad \lambda_n = \sqrt{\frac{t_{n+1} - t_{n-1}}{2s}}$$

is a frame with frame bounds $A \geqslant (1 - \delta/s)^2$ and $B \leqslant (1 + \delta/s)^2$. The amplitude factor λ_n compensates for the increase of sample density relatively to s. The reconstruction of f requires inverting the frame operator $\Phi f[n] = \langle f(u), \lambda_n, \phi_s(u - t_n) \rangle$.

5.1.2 Dual Frame and Pseudo Inverse

The reconstruction of f from its frame coefficients $\Phi f[n]$ is calculated with a pseudo inverse also called Moore-Penrose pseudo inverse. This pseudo inverse is a bounded operator that implements a dual-frame reconstruction. For Riesz bases, this dual frame is a biorthogonal basis.

For any operator U, we denote by **Im**U the image space of all Uf and by **Null**U the null space of all h, such that $Uh = 0$.

Theorem 5.3. If $\{\phi_n\}_{n \in \Gamma}$ is a frame but not a Riesz basis, then Φ admits an infinite number of left inverses.

Proof. We know that $\textbf{Null}\Phi^* = (\textbf{Im}\Phi)^\perp$ is the orthogonal complement of $\textbf{Im}\Phi$ in $\ell^2(\Gamma)$ (Exercise 5.7). If Φ is a frame and not a Riesz basis, then $\{\phi_n\}_{n \in \Gamma}$ is linearly dependent, so there exists $a \in \textbf{Null}\Phi^* = (\textbf{Im}\Phi)^\perp$ with $a \neq 0$.

A frame operator Φ is injective (one to one). Indeed, the frame inequality (5.2) guarantees that $\Phi f = 0$ implies $f = 0$. Its restriction to $\textbf{Im}\Phi$ is thus invertible, which means that Φ admits a left inverse. There is an infinite number of left inverses since the restriction of a left inverse to $(\textbf{Im}\Phi)^\perp \neq \{0\}$ may be any arbitrary linear operator. ∎

The more redundant the frame $\{\phi_n\}_{n \in \Gamma}$, the larger the orthogonal complement $(\textbf{Im}\Phi)^\perp$ of $\textbf{Im}\Phi$ in $\ell^2(\Gamma)$. The pseudo inverse, written as Φ^+, is defined as the left inverse that is zero on $(\textbf{Im}\Phi)^\perp$:

$$\forall f \in \textbf{H}, \quad \Phi^+ \Phi f = f \quad \text{and} \quad \forall a \in (\textbf{Im}\Phi)^\perp, \quad \Phi^+ a = 0. \tag{5.9}$$

Theorem 5.4 computes this pseudo inverse.

Theorem 5.4: *Pseudo Inverse.* If Φ is a frame operator, then $\Phi^*\Phi$ is invertible and the pseudo inverse satisfies

$$\Phi^+ = (\Phi^*\Phi)^{-1}\Phi^*. \tag{5.10}$$

Proof. The frame condition in (5.4) is rewritten as

$$\forall f \in \textbf{H}, \quad A \|f\|^2 \leqslant \langle \Phi^*\Phi f, f \rangle \leqslant B \|f\|^2.$$

The result is that $\Phi^*\Phi$ is an injective self-adjoint operator: $\Phi^*\Phi f = 0$ if and only if $f = 0$. It is therefore invertible. For all $f \in \textbf{H}$,

$$\Phi^+ \Phi f = (\Phi^*\Phi)^{-1}\Phi^*\Phi f = f,$$

so Φ^+ is a left inverse. Since $(\textbf{Im}\Phi)^\perp = \textbf{Null}\Phi^*$, it results that $\Phi^+ a = 0$ for any $a \in (\textbf{Im}\Phi)^\perp = \textbf{Null}\Phi^*$. Since this left inverse vanishes on $(\textbf{Im}\Phi)^\perp$, it is the pseudo inverse. ∎

Dual Frame

The pseudo inverse of a frame operator implements a reconstruction with a dual frame, which is specified by Theorem 5.5.

Theorem 5.5. Let $\{\phi_n\}_{n\in\Gamma}$ be a frame with bounds $0<A\leqslant B$. The dual operator defined by

$$\forall n\in\Gamma, \quad \tilde{\Phi}f[n]=\langle f,\tilde{\phi}_n\rangle \quad \text{with} \quad \tilde{\phi}_n=(\Phi^*\Phi)^{-1}\phi_n \tag{5.11}$$

satisfies $\tilde{\Phi}^*=\Phi^+$, and thus

$$f=\sum_{n\in\Gamma}\langle f,\phi_n\rangle\,\tilde{\phi}_n=\sum_{n\in\Gamma}\langle f,\tilde{\phi}_n\rangle\,\phi_n. \tag{5.12}$$

It defines a dual frame as

$$\forall f\in\mathbf{H}, \quad \frac{1}{B}\|f\|^2\leqslant\sum_{n\in\Gamma}|\langle f,\tilde{\phi}_n\rangle|^2\leqslant\frac{1}{A}\|f\|^2. \tag{5.13}$$

If the frame is tight (i.e., $A=B$), then $\tilde{\phi}_n=A^{-1}\phi_n$.

Proof. The dual operator can be written as $\tilde{\Phi}=\Phi(\Phi^*\Phi)^{-1}$. Indeed,

$$\tilde{\Phi}f[n]=\langle f,\tilde{\phi}_n\rangle=\langle f,(\Phi^*\Phi)^{-1}\phi_n\rangle=\langle(\Phi^*\Phi)^{-1}f,\phi_n\rangle=\Phi(\Phi^*\Phi)^{-1}f.$$

Thus, we derive from (5.10) that its adjoint is the pseudo inverse of Φ:

$$\tilde{\Phi}^*=(\Phi^*\Phi)^{-1}\Phi^*=\Phi^+.$$

It results that $\Phi^+\Phi=\tilde{\Phi}^*\Phi=\text{Id}$ and thus that $\Phi^*\tilde{\Phi}=\text{Id}$, which proves (5.12).

Let us now prove the frame bounds (5.13). Frame conditions are rewritten in (5.4):

$$\forall f\in\mathbf{H}, \quad A\|f\|^2\leqslant\langle\Phi^*\Phi f,f\rangle\leqslant B\|f\|^2. \tag{5.14}$$

Lemma 5.1 applied to $L=\Phi^*\Phi$ proves that

$$\forall f\in\mathbf{H}, \quad B^{-1}\|f\|^2\leqslant\langle(\Phi^*\Phi)^{-1}f,f\rangle\leqslant A^{-1}\|f\|^2. \tag{5.15}$$

Since for any $f\in\mathbf{H}$

$$\|\tilde{\Phi}f\|^2=\langle\Phi(\Phi^*\Phi)^{-1}f,\Phi(\Phi^*\Phi)^{-1}f\rangle=\langle f,(\Phi^*\Phi)^{-1}f\rangle,$$

the dual-frame bounds (5.13) are derived from (5.15).

If $A=B$, then $\langle\Phi^*\Phi f,f\rangle=A\|f\|^2$. Thus, the spectrum of $\Phi^*\Phi$ is reduced to A and therefore $\Phi^*\Phi=A\,\text{Id}$. As a result, $\tilde{\phi}_n=(\Phi^*\Phi)^{-1}\phi_n=A^{-1}\phi_n$.

Lemma 5.1. If L is a self-adjoint operator such that there exist $B\geqslant A>0$ satisfying

$$\forall f\in\mathbf{H}, \quad A\|f\|^2\leqslant\langle Lf,f\rangle\leqslant B\|f\|^2, \tag{5.16}$$

then L is invertible and

$$\forall f\in\mathbf{H}, \quad \frac{1}{B}\|f\|^2\leqslant\langle L^{-1}f,f\rangle\leqslant\frac{1}{A}\|f\|^2. \tag{5.17}$$

In finite dimensions, since L is self-adjoint we know that it is diagonalized in an orthonormal basis. The inequality (5.16) proves that its eigenvalues are between A and B. It is therefore invertible with eigenvalues between B^{-1} and A^{-1}, which proves (5.17). In a Hilbert space of infinite dimension, we prove that same result on the supremum and infimum of the spectrum by growing the space dimension, and computing the limit of the largest and smallest eigenvalues when the space dimension tends to infinity.   ■

This theorem proves that f is reconstructed from frame coefficients $\Phi f[n] = \langle f, \phi_n \rangle$ with the dual frame $\{\tilde{\phi}_n\}_{n \in \Gamma}$. The synthesis coefficients of f in $\{\phi_n\}_{n \in \Gamma}$ are the dual-frame coefficients $\tilde{\Phi} f[n] = \langle f, \phi_n \rangle$. If the frame is tight, then both decompositions are identical:

$$f = \frac{1}{A} \sum_{n \in \Gamma} \langle f, \phi_n \rangle \, \phi_n. \tag{5.18}$$

Biorthogonal Bases

A Riesz basis is a frame of vectors that are linearly independent, which implies that $\mathbf{Im}\Phi = \ell^2(\Gamma)$, so its dual frame is also linearly independent. Inserting $f = \phi_p$ in (5.12) yields

$$\phi_p = \sum_{n \in \Gamma} \langle \phi_p, \tilde{\phi}_n \rangle \, \phi_n,$$

and the linear independence implies that

$$\langle \phi_p, \tilde{\phi}_n \rangle = \delta[p - n].$$

Thus, dual Riesz bases are biorthogonal families of vectors. If the basis is normalized (i.e., $\|\phi_n\| = 1$), then

$$A \leqslant 1 \leqslant B. \tag{5.19}$$

This is proved by inserting $f = \phi_p$ in the frame inequality (5.13):

$$\frac{1}{B} \|\phi_p\|^2 \leqslant \sum_{n \in \Gamma} |\langle \phi_p, \tilde{\phi}_n \rangle|^2 = 1 \leqslant \frac{1}{A} \|\phi_p\|^2.$$

5.1.3 Dual-Frame Analysis and Synthesis Computations

Suppose that $\{\phi_n\}_{n \in \Gamma}$ is a frame of a subspace $\mathbf{V}$ of the whole signal space. The best linear approximation of f in $\mathbf{V}$ is the orthogonal projection of f in $\mathbf{V}$. Theorem 5.6 shows that this orthogonal projection is computed with the dual frame. Two iterative numerical algorithms are described to implement such computations.

Theorem 5.6. Let $\{\phi_n\}_{n \in \Gamma}$ be a frame of $\mathbf{V}$, and $\{\tilde{\phi}_n\}_{n \in \Gamma}$ it's dual frame in $\mathbf{V}$. The orthogonal projection of $f \in \mathbf{H}$ in $\mathbf{V}$ is

$$P_{\mathbf{V}} f = \sum_{n \in \Gamma} \langle f, \phi_n \rangle \, \tilde{\phi}_n = \sum_{n \in \Gamma} \langle f, \tilde{\phi}_n \rangle \, \phi_n. \tag{5.20}$$

Proof. Since both frames are dual in $\mathbf{V}$, if $f \in \mathbf{V}$, then, (5.12) proves that the operator $P_{\mathbf{V}}$ defined in (5.20) satisfies $P_{\mathbf{V}} f = f$. To prove that it is an orthogonal projection it is sufficient to verify that if $f \in \mathbf{H}$ then $\langle f - P_{\mathbf{V}} f, \phi_p \rangle = 0$ for all $p \in \Gamma$. Indeed,

$$\langle f - P_{\mathbf{V}} f, \phi_p \rangle = \langle f, \phi_p \rangle - \sum_{n \in \Gamma} \langle f, \phi_n \rangle \langle \tilde{\phi}_n, \phi_p \rangle = 0$$

because the dual-frame property implies that $\sum_{n \in \Gamma} \langle \tilde{\phi}_n, \phi_p \rangle \phi_n = \phi_p$. ∎

If Γ is finite, then $\{\phi_n\}_{n \in \Gamma}$ is necessarily a frame of the space $\mathbf{V}$ it generates, and (5.20) reconstructs the best linear approximation of f in $\mathbf{V}$. This result is particularly important for approximating signals from a finite set of vectors.

Since Φ is not a frame of the whole signal space $\mathbf{H}$, but of a subspace $\mathbf{V}$ then Φ is only invertible on this subspace and the pseudo-inverse definition becomes:

$$\forall f \in \mathbf{V}, \quad \Phi^+ \Phi f = f \quad \text{and} \quad \forall a \in (\mathbf{Im}\Phi)^\perp, \quad \Phi^+ a = 0. \tag{5.21}$$

Let $\Phi_{\mathbf{V}}$ be the restriction of Φ to $\mathbf{V}$. The operator $\Phi^* \Phi_{\mathbf{V}}$ is invertible on $\mathbf{V}$ and we write $(\Phi^* \Phi_{\mathbf{V}})^{-1}$ its inverse. Similar to (5.10), we verify that $\Phi^+ = (\Phi^* \Phi_{\mathbf{V}})^{-1} \Phi^*$.

Dual Synthesis
In a dual synthesis problem, the orthogonal projection is computed from the frame coefficients $\{\Phi f[n] = \langle f, \phi_n \rangle\}_{n \in \Gamma}$ with the dual-frame synthesis operator:

$$P_{\mathbf{V}} f = \tilde{\Phi}^* \Phi f = \sum_{n \in \Gamma} \langle f, \phi_n \rangle \tilde{\phi}_n. \tag{5.22}$$

If the frame $\{\phi_n\}_{n \in \Gamma}$ does not depend on the signal f, then the dual-frame vectors are precomputed with (5.11):

$$\forall n \in \Gamma, \quad \tilde{\phi}_n = (\Phi^* \Phi_{\mathbf{V}})^{-1} \phi_n, \tag{5.23}$$

and the dual synthesis is solved directly with (5.22). In many applications, the frame vectors $\{\phi_n\}_{n \in \Gamma}$ depend on the signal f, in which case the dual-frame vectors $\tilde{\phi}_n$ cannot be computed in advance, and it is highly inefficient to compute them. This is the case when coefficients $\{\langle f, \phi_n \rangle\}_{n \in \Gamma}$ are selected in a redundant transform, to build a sparse signal representation. For example, the time-frequency ridge vectors in Sections 4.4.2 and 4.4.3 are selected from the local maxima of f in highly redundant windowed Fourier or wavelet transforms.

The transform coefficients Φf are known and we must compute

$$P_{\mathbf{V}} f = \tilde{\Phi}^* \Phi f = (\Phi^* \Phi_{\mathbf{V}})^{-1} \Phi^* \Phi f.$$

A dual-synthesis algorithm computes first

$$y = \Phi^* \Phi f = \sum_{n \in \Gamma} \langle f, \phi_n \rangle \phi_n \in \mathbf{V}$$

and then derives $P_{\mathbf{V}} f = L^{-1} y = z$ by applying the inverse of the symmetric operator $L = \Phi^* \Phi_{\mathbf{V}}$ to y, with

$$\forall h \in \mathbf{V}, \quad Lh = \sum_{n \in \Gamma} \langle h, \phi_n \rangle \, \phi_n. \tag{5.24}$$

The eigenvalues of L are between A and B.

Dual Analysis

In a dual analysis, the orthogonal projection $P_{\mathbf{V}} f$ is computed from the frame vectors $\{\phi_n\}_{n \in \Gamma}$ with the dual-frame analysis operator $\tilde{\Phi} f[n] = \langle f, \tilde{\phi}_n \rangle$:

$$P_{\mathbf{V}} f = \Phi^* \, \tilde{\Phi} f = \sum_{n \in \Gamma} \langle f, \tilde{\phi}_n \rangle \, \phi_n. \tag{5.25}$$

If $\{\phi_n\}_{n \in \Gamma}$ does not depend upon f then $\{\tilde{\phi}_n\}_{n \in \Gamma}$ is precomputed with (5.23). The $\{\phi_n\}_{n \in \Gamma}$ may also be selected adaptively from a larger dictionary, to provide a sparse approximation of f. Computing the orthogonal projection $P_{\mathbf{V}} f$ is called a *backprojection*. In Section 12.3, matching pursuits implement this backprojection.

When $\{\phi_n\}_{n \in \Gamma}$ depends on f, computing the dual frame is inefficient. The dual coefficient $a[n] = \tilde{\Phi} f[n]$ is calculated directly, as well as

$$P_{\mathbf{V}} f = \Phi^* a = \sum_{n \in \Gamma} a[n] \, \phi_n. \tag{5.26}$$

Since $\Phi P_{\mathbf{V}} f = \Phi f$, we have $\Phi \Phi^* a = \Phi f$. Let $\Phi^*_{\mathbf{Im}\Phi}$ be the restriction of Φ^* to $\mathbf{Im}\Phi$. Since $\Phi \Phi^*_{\mathbf{Im}\Phi}$ is invertible on $\mathbf{Im}\Phi$

$$a = (\Phi \Phi^*_{\mathbf{Im}\Phi})^{-1} \Phi f.$$

Thus, the dual-analysis algorithm computes $y = \Phi f = \{\langle f, \phi_n \rangle\}_{n \in \Gamma}$ and derives the dual coefficients $a = L^{-1} y = z$ by applying the inverse of the Gram operator $L = \Phi \Phi^*_{\mathbf{Im}\Phi}$ to y, with

$$Lh[n] = \sum_{p \in \Gamma} h[n] \, \langle \phi_n, \phi_p \rangle. \tag{5.27}$$

The eigenvalues of L are also between A and B. The orthogonal projection of f is recovered with (5.26).

Richardson Inversion of Symmetric Operators

The key computational step of a dual-analysis or a dual-synthesis problem is to compute $z = L^{-1} y$, where L is a symmetric operator with eigenvalues that are between A and B. Theorems 5.7 and 5.8 describe two iterative algorithms with exponential convergence. The *Richardson iteration procedure* is simpler but requires knowing the frame bounds A and B. *Conjugate gradient* iterations converge more quickly when B/A is large, and do not require knowing the values of A and B.

Theorem 5.7. To compute $z = L^{-1}y$, let z_0 be an initial value and $\gamma > 0$ be a relaxation parameter. For any $k > 0$, define

$$z_k = z_{k-1} + \gamma \, (y - L z_{k-1}). \tag{5.28}$$

If

$$\delta = \max \{|1 - \gamma A|, \, |1 - \gamma B|\} < 1, \tag{5.29}$$

then

$$\|z - z_k\| \leqslant \delta^k \, \|z - z_0\|, \tag{5.30}$$

and therefore $\lim_{k \to +\infty} z_k = z$.

Proof. The induction equation (5.28) can be rewritten as

$$z - z_k = z - z_{k-1} - \gamma \, L(z - z_{k-1}).$$

Let

$$R = Id - \gamma \, L,$$

$$z - z_k = R(z - z_{k-1}) = R^k (z - z_0). \tag{5.31}$$

Since the eigenvalues of L are between A and B,

$$A \, \|z\|^2 \leqslant \langle Lz, z \rangle \leqslant B \, \|z\|^2.$$

This implies that $R = I - \gamma L$ satisfies

$$|\langle Rz, z \rangle| \leqslant \delta \, \|z\|^2,$$

where δ is given by (5.29). Since R is symmetric, this inequality proves that $\|R\| \leqslant \delta$. Thus, we derive (5.30) from (5.31). The error $\|z - z_k\|$ clearly converges to zero if $\delta < 1$. ∎

The convergence is guaranteed for all initial values z_0. If an estimation z_0 of the solution z is known, then this estimation can be chosen; otherwise, z_0 is often set to 0. For frame inversion, the Richardson iteration algorithm is sometimes called the *frame algorithm* [19]. The convergence rate is maximized when δ is minimum:

$$\delta = \frac{B - A}{B + A} = \frac{1 - A/B}{1 + A/B},$$

which corresponds to the relaxation parameter

$$\gamma = \frac{2}{A + B}. \tag{5.32}$$

The algorithm converges quickly if A/B is close to 1. If A/B is small then

$$\delta \approx 1 - 2 \frac{A}{B}. \tag{5.33}$$

The inequality (5.30) proves that we obtain an error smaller than ε for a number n of iterations, which satisfies

$$\frac{\|z - z_k\|}{\|z - z_0\|} \leqslant \delta^k = \varepsilon.$$

Inserting (5.33) gives

$$k \approx \frac{\log_e \varepsilon}{\log_e(1 - 2A/B)} \approx \frac{-B}{2A} \log_e \varepsilon. \tag{5.34}$$

Therefore, the number of iterations increases proportionally to the frame-bound ratio B/A.

The exact values of A and B are often not known, and A is generally more difficult to compute. The upper frame bound is $B = \|\Phi \, \Phi^*\|_S = \|\Phi^* \, \Phi\|_S$. If we choose

$$\gamma < 2 \, \|\Phi \, \Phi^*\|_S^{-1}, \tag{5.35}$$

then (5.29) shows that the algorithm is guaranteed to converge, but the convergence rate depends on A. Since $0 < A \leqslant B$, the optimal relaxation parameter γ in (5.32) is in the range $\|\Phi \, \Phi^*\|_S^{-1} \leqslant \gamma < 2 \, \|\Phi \, \Phi^*\|_S^{-1}$.

Conjugate-Gradient Inversion

The conjugate-gradient algorithm computes $z = L^{-1}y$ with a gradient descent along orthogonal directions with respect to the norm induced by the symmetric operator L:

$$\|z\|_L^2 = \|Lz\|^2. \tag{5.36}$$

This L norm is used to estimate the error. Gröchenig's [287] implementation of the conjugate-gradient algorithm is given by Theorem 5.8.

Theorem 5.8: *Conjugate Gradient.* To compute $z = L^{-1}y$, we initialize

$$z_0 = 0, \quad r_0 = p_0 = y, \quad p_{-1} = 0. \tag{5.37}$$

For any $k \geqslant 0$, we define by induction:

$$\lambda_k = \frac{\langle r_k, p_k \rangle}{\langle p_k, Lp_k \rangle} \tag{5.38}$$

$$z_{k+1} = z_k + \lambda_k p_k \tag{5.39}$$

$$r_{k+1} = r_k - \lambda_k Lp_k \tag{5.40}$$

$$p_{k+1} = Lp_k - \frac{\langle Lp_k, Lp_k \rangle}{\langle p_k, Lp_k \rangle} p_k - \frac{\langle Lp_k, Lp_{k-1} \rangle}{\langle p_{k-1}, Lp_{k-1} \rangle} p_{k-1}. \tag{5.41}$$

If $\sigma = \frac{\sqrt{B} - \sqrt{A}}{\sqrt{B} + \sqrt{A}}$, then

$$\|z - z_k\|_L \leqslant \frac{2\sigma^k}{1 + \sigma^{2k}} \|z\|_L, \tag{5.42}$$

and therefore $\lim_{k \to +\infty} z_k = z$.

Proof. We give the main steps of the proof as outlined by Gröchenig [287].

Step 1. Let $\mathbf{U}_k$ be the subspace generated by $\{L^j z\}_{1 \leqslant j \leqslant k}$. By induction on k, we derive from (5.41) that $p_j \in \mathbf{U}_k$, for $j < k$.

Step 2. We prove by induction that $\{p_j\}_{0 \leqslant j < k}$ is an orthogonal basis of $\mathbf{U}_k$ with respect to the inner product $\langle z, h \rangle_L = \langle z, Lh \rangle$. Assuming that $\langle p_k, Lp_j \rangle = 0$, for $j \leqslant k-1$, it can be shown that $\langle p_{k+1}, Lp_j \rangle = 0$, for $j \leqslant k$.

Step 3. We verify that z_k is the orthogonal projection of z onto $\mathbf{U}_k$ with respect to $\langle ., . \rangle_L$, which means that

$$\forall g \in \mathbf{U}_k, \quad \|z - g\|_L \geqslant \|z - z_k\|_L.$$

Since $z_k \in \mathbf{U}_k$, this requires proving that $\langle z - z_k, p_j \rangle_L = 0$, for $j < k$.

Step 4. We compute the orthogonal projection of z in embedded spaces $\mathbf{U}_k$ of dimension k, and one can verify that $\lim_{k \to +\infty} \|z - z_k\|_L = 0$. The exponential convergence (5.42) is proved in [287]. ∎

As opposed to the Richardson algorithm, the initial value z_0 must be set to 0. As in the Richardson iteration algorithm, the convergence is slower when A/B is small. In this case,

$$\sigma = \frac{1 - \sqrt{A/B}}{1 + \sqrt{A/B}} \approx 1 - 2\sqrt{\frac{A}{B}}.$$

The upper bound (5.42) proves that we obtain a relative error

$$\frac{\|z - z_k\|_L}{\|z\|_L} \leqslant \varepsilon$$

for a number of iterations

$$k \approx \frac{\log_e \frac{\varepsilon}{2}}{\log_e \sigma} \approx \frac{-\sqrt{B}}{2\sqrt{A}} \log_e \frac{\varepsilon}{2}.$$

Comparing this result with (5.34) shows that when A/B is small, the conjugate-gradient algorithm needs much less iterations than the Richardson iteration algorithm to compute $z = L^{-1}y$ at a fixed precision.

5.1.4 Frame Projector and Reproducing Kernel

Frame redundancy is useful in reducing noise added to the frame coefficients. The vector computed with noisy frame coefficients is projected on the image of Φ to reduce the amplitude of the noise. This technique is used for high-precision analog-to-digital conversion based on oversampling. The following theorem specifies the orthogonal projector on $\mathbf{Im}\Phi$.

Theorem 5.9: *Reproducing Kernel*. Let $\{\phi_n\}_{n \in \Gamma}$ be a frame of $\mathbf{H}$ or of a subspace $\mathbf{V}$. The orthogonal projection from $\ell^2(\Gamma)$ onto $\mathbf{Im}\Phi$ is

$$Pa[n] = \Phi\,\Phi^+ a[n] = \sum_{p \in \Gamma} a[p]\,\langle \tilde{\phi}_p, \phi_n \rangle. \tag{5.43}$$

Coefficients $a \in \ell^2(\Gamma)$ are frame coefficients $a \in \mathbf{Im}\,\Phi$ if and only if they satisfy the reproducing kernel equation

$$a[n] = \Phi\,\Phi^+ a[n] = \sum_{p \in \Gamma} a[p]\,\langle \tilde{\phi}_p, \phi_n \rangle. \tag{5.44}$$

Proof. If $a \in \mathbf{Im}\,\Phi$, then $a = \Phi f$ and

$$Pa = \Phi\,\Phi^+ \Phi f = \Phi f = a.$$

If $a \in (\mathbf{Im}\,\Phi)^\perp$, then $Pa = 0$ because $\Phi^+ a = 0$. This proves that P is an orthogonal projector on $\mathbf{Im}\,\Phi$. Since $\Phi f[n] = \langle f, \phi_n \rangle$ and $\Phi^+ a = \sum_{p \in \Gamma} a[p]\,\tilde{\phi}_p$, we derive (5.43).

A vector $a \in \ell^2(\Gamma)$ belongs to $\mathbf{Im}\,\Phi$ if and only if $a = Pa$, which proves (5.44). ∎

The reproducing kernel equation (5.44) expresses the redundancy of frame coefficients. If the frame is not redundant and is a Riesz basis, then $\langle \tilde{\phi}_p, \phi_n \rangle = 0$, so this equation vanishes.

Noise Reduction
Suppose that each frame coefficient $\Phi f[n]$ is contaminated by an additive noise $W[n]$, which is a random variable. Applying the projector P gives

$$P(\Phi f + W) = \Phi f + PW,$$

with

$$PW[n] = \sum_{p \in \Gamma} W[p]\,\langle \tilde{\phi}_p, \phi_n \rangle.$$

Since P is an orthogonal projector, $\|PW\| \leqslant \|W\|$. This projector removes the component of W that is in $(\mathbf{Im}\,\Phi)^\perp$. Increasing the redundancy of the frame reduces the size of $\mathbf{Im}\,\Phi$ and thus increases $(\mathbf{Im}\,\Phi)^\perp$, so a larger portion of the noise is removed. If W is a white noise, its energy is uniformly distributed in the space $\ell^2(\Gamma)$. Theorem 5.10 proves that its energy is reduced by at least A if the frame vectors are normalized.

Theorem 5.10. Suppose that $\|\phi_n\| = C$, for all $n \in \Gamma$. If W is a zero-mean white noise of variance $E\{|W[n]|^2\} = \sigma^2$, then

$$E\{|PW[n]|^2\} \leqslant \frac{\sigma^2\,C^2}{A}. \tag{5.45}$$

If the frame is tight then this inequality is an equality.

Proof. Let us compute

$$E\{|PW[n]|^2\} = E\left\{ \left(\sum_{p \in \Gamma} W[p]\,\langle \tilde{\phi}_p, \phi_n \rangle \right) \left(\sum_{l \in \Gamma} W^*[l]\,\langle \tilde{\phi}_l, \phi_n \rangle^* \right) \right\}.$$

Since W is white,

$$E\{W[p]\, W^*[l]\} = \sigma^2\, \delta[p - l],$$

and therefore,

$$E\{|PW[n]|^2\} = \sigma^2 \sum_{p \in \Gamma} |\langle \tilde{\phi}_p, \phi_n \rangle|^2 \leqslant \frac{\sigma^2\, \|\phi_n\|^2}{A} = \frac{\sigma^2\, C^2}{A}.$$

The last inequality is an equality if the frame is tight. ∎

Oversampling

This noise-reduction strategy is used by high-precision analog-to-digital converters. After a low-pass filter, a band-limited analog signal $f(t)$ is uniformly sampled and quantized. In hardware, it is often easier to increase the sampling rate rather than the quantization precision. Increasing the sampling rate introduces a redundancy between the sample values of the band-limited signal. Thus, these samples can be interpreted as frame coefficients. For a wide range of signals it has been shown that the quantization error is nearly a white noise [277]. Thus, it can be significantly reduced by a frame projector, which in this case is a low-pass convolution operator (Exercise 5.16).

The noise can be further reduced if it is not white and if its energy is better concentrated in $(\mathbf{Im}\Phi)^\perp$. This can be done by transforming the quantization noise into a noise that has energy mostly concentrated at high frequencies. Sigma–delta modulators produce such quantization noises by integrating the signal before its quantization [89]. To compensate for the integration, the quantized signal is differentiated. This differentiation increases the energy of the quantized noise at high frequencies and reduces its energy at low frequencies [456].

5.1.5 Translation-Invariant Frames

Section 4.1 introduces translation-invariant dictionaries obtained by translating a family of generators $\{\phi_n\}_{n \in \Gamma}$, which are used to construct translation-invariant signal representations. In multiple dimensions for $\phi_n \in \mathbf{L}^2(\mathbb{R}^d)$, the resulting dictionary can be written $\mathcal{D} = \{\phi_{u,n}(x)\}_{n \in \Gamma, u \in \mathbb{R}^d}$, with $\phi_{u,n}(x) = \lambda_{u,n}\,\phi_n(x - u)$. In a translation-invariant wavelet dictionary, the generators are obtained by dilating a wavelet $\psi(t)$ with scales s_n: $\phi_n(t) = s_n^{-1/2}\psi(x/s_n)$. In a window Fourier dictionary, the generators are obtained by modulating a window $g(x)$ at frequencies ξ_n: $\phi_n(x) = e^{i\xi_n x} g(x)$.

The decomposition coefficients of f in $\mathcal{D}$ are convolution products

$$\Phi f(u, n) = \langle f, \phi_{u,n} \rangle = \lambda_{u,n} f \star \bar{\phi}_n(u) \quad \text{with} \quad \bar{\phi}_n(x) = \phi_n^*(-x). \tag{5.46}$$

Suppose that Γ is a countable set. The overall index set $\mathbb{R}^d \times \Gamma$ is not countable, so the dictionary $\mathcal{D}$ cannot strictly speaking be considered as a frame. However, if we

consider the overall energy of dictionary coefficients, calculated with a sum and a multidimensional integral

$$\sum_{n\in\Gamma} \|\Phi f(u,n)\|^2 = \sum_{n\in\Gamma} \int |\Phi f(u,n)| \, du,$$

and if there exist two constants $A>0$ and $B>0$ such that for all $f \in \mathbf{L}^2(\mathbb{R})$,

$$A\,\|f\|^2 \leqslant \sum_{n\in\Gamma} \|\Phi f(u,n)\|^2 \leqslant B\,\|f\|^2, \tag{5.47}$$

then the frame theory results of the previous section apply. Thus, with an abuse of language, such translation-invariant dictionaries will also be called frames. Theorem 5.11 proves that the frame condition (5.47) is equivalent to a condition on the Fourier transform $\hat{\phi}_n(\omega)$ of the generators.

Theorem 5.11. If there exist two constants $B \geqslant A > 0$ such that for almost all ω in $\mathbb{R}^d$

$$A \leqslant \sum_{n\in\Gamma} |\hat{\phi}_n(\omega)|^2 \leqslant B, \tag{5.48}$$

then the frame inequality (5.47) is valid for all $f \in \mathbf{L}^2(\mathbb{R}^d)$. Any $\{\tilde{\phi}_n\}_{n\in\Gamma}$ that satisfies for almost all ω in $\mathbb{R}^d$

$$\sum_{n\in\Gamma} \hat{\phi}_n^*(\omega)\,\widehat{\tilde{\phi}}_n(\omega) = 1, \tag{5.49}$$

defines a left inverse

$$f(t) = \sum_{n\in\Gamma} \Phi f(.,n) \star \tilde{\phi}_n(t). \tag{5.50}$$

The pseudo inverse (dual frame) is implemented by

$$\widehat{\tilde{\phi}}_n(\omega) = \frac{\hat{\phi}_n(\omega)}{\sum_{n\in\Gamma} |\hat{\phi}_n(\omega)|^2}. \tag{5.51}$$

Proof. The frame condition (5.47) means that $\Phi^*\Phi$ has a spectrum bounded by A and B. It results from (5.46) that

$$\Phi^*\Phi f(x) = f \star \Big(\sum_{n\in\Gamma} \phi_n \star \bar{\phi}_n\Big)(x). \tag{5.52}$$

The spectrum of this convolution operator is given by the Fourier transform of $\sum_{n\in\Gamma} \phi_n \star \bar{\phi}_n(x)$, which is $\sum_{n\in\Gamma} |\hat{\phi}_n(\omega)|^2$. Thus, the frame inequality (5.47) is equivalent to condition '(5.48).

Equation (5.50) is proved by taking the Fourier transform on both sides and inserting (5.49).

Theorem 5.5 proves that the dual-frame vectors implementing the pseudo inverse are $\tilde{\phi}_{n,u} = (\Phi^*\Phi)^{-1}\phi_{n,u}$. Since $\Phi^*\Phi$ is the convolution operator (5.52), its inverse is calculated by inverting its transfer function, which yields (5.51). ∎

For wavelet or windowed Fourier translation-invariant dictionaries, the theorem condition (5.48) becomes a condition on the Fourier transform of the wavelet $\hat{\psi}(\omega)$ or on the Fourier transform of the window $\hat{g}(\omega)$. As explained in Sections 5.3 and 5.4, more conditions are needed to obtain a frame by discretizing the translation parameter u.

Discrete Translation-Invariant Frames

For finite-dimensional signals $f[n] \in \mathbb{C}^N$ a circular translation-invariant frame is obtained with a periodic shift modulo N of a finite number of generators $\{\phi_m[n]\}_{0 \leqslant m < M}$:

$$\mathcal{D} = \{\phi_{m,p}[n] = \phi_m[(n-p)\mathrm{mod}N]\}_{0 \leqslant m < M, 0 \leqslant p < N}.$$

Such translation-invariant frames appear in Section 11.2.3 to define translation-invariant thresholding estimators for noise removal. Similar to Theorem 5.11, Theorem 5.12 gives a necessary and sufficient condition on the discrete Fourier transform $\hat{\phi}_m[k] = \sum_{n=0}^{N-1} \phi_m[n]\mathrm{e}^{-i2\pi k/N}$ of the generators $\phi_m[n]$ to obtain a frame.

Theorem 5.12. A circular translation-invariant dictionary $\mathcal{D} = \{\phi_{m,p}[n]\}_{0 \leqslant m < M, 0 \leqslant n < N}$ is a frame with frame bounds $0 < A \leqslant B$ if and only if

$$\forall 0 \leqslant k < N \; A \leqslant \sum_{m=0}^{M-1} |\hat{\phi}_m[k]|^2 \leqslant B. \tag{5.53}$$

The proof proceeds essentially like the proof of Theorem 5.11, and is left in Exercise 5.8.

5.2 TRANSLATION-INVARIANT DYADIC WAVELET TRANSFORM

The continuous wavelet transform of Section 4.3 decomposes one-dimensional signals $f \in \mathbf{L}^2(\mathbb{R})$ over a dictionary of translated and dilated wavelets

$$\psi_{u,s}(t) = \frac{1}{\sqrt{s}} \, \psi\left(\frac{t-u}{s}\right).$$

Translation-invariant wavelet dictionaries are constructed by sampling the scale parameter s along an exponential sequence $\{\nu^j\}_{j \in \mathbb{Z}}$, while keeping all translation parameters u. We choose $\nu = 2$ to simplify computer implementations:

$$\mathcal{D} = \left\{\psi_{u,2^j}(t) = \frac{1}{\sqrt{2^j}} \, \psi\left(\frac{t-u}{2^j}\right)\right\}_{u \in \mathbb{R}, j \in \mathbb{Z}}.$$

The resulting dyadic wavelet transform of $f \in \mathbf{L}^2(\mathbb{R})$ is defined by

$$Wf(u, 2^j) = \langle f, \psi_{u,2^j} \rangle = \int_{-\infty}^{+\infty} f(t) \frac{1}{\sqrt{2^j}} \, \psi\left(\frac{t-u}{2^j}\right) dt = f \star \bar{\psi}_{2^j}(u), \tag{5.54}$$

with

$$\bar{\psi}_{2^j}(t) = \psi_{2^j}(-t) = \frac{1}{2^j}\, \psi\left(\frac{-t}{2^j}\right).$$

Translation-invariant dyadic wavelet transforms are used in pattern-recognition applications and for denoising with translation-invariant wavelet thresholding estimators, as explained in Section 11.3.1. Fast computations with filter banks are presented in the next two sections.

Theorem 5.11 on translation-invariant dictionaries can be applied to the multiscale wavelet generators $\phi_n(t) = 2^{-j/2}\,\psi_{2^j}(t)$. Since $\hat{\phi}_n(\omega) = \hat{\psi}(2^j\omega)$, the Fourier condition (5.48) means that there exist two constants $A > 0$ and $B > 0$ such that

$$\forall \omega \in \mathbb{R} - \{0\}, \quad A \leq \sum_{j=-\infty}^{+\infty} |\hat{\psi}(2^j\omega)|^2 \leq B, \tag{5.55}$$

and since $\Phi f(u, n) = 2^{-j/2} W f(u, n)$, Theorem 5.11 proves the frame inequality

$$A \|f\|^2 \leq \sum_{j=-\infty}^{+\infty} \frac{1}{2^j}\, \|W f(u, 2^j)\|^2 \leq B \|f\|^2. \tag{5.56}$$

This shows that if the frequency axis is completely covered by dilated dyadic wavelets, as shown in Figure 5.1, then a dyadic wavelet transform defines a complete and stable representation.

Moreover, if $\tilde{\psi}$ satisfies

$$\forall \omega \in \mathbb{R} - \{0\}, \quad \sum_{j=-\infty}^{+\infty} \hat{\psi}^*(2^j\omega)\, \widehat{\tilde{\psi}}(2^j\omega) = 1, \tag{5.57}$$

then (5.50) applied to $\tilde{\phi}_n(t) = 2^{-j}\tilde{\psi}(2^{-j}t)$ proves that

$$f(t) = \sum_{j=-\infty}^{+\infty} \frac{1}{2^j}\, W f(., 2^j) \star \tilde{\psi}_{2^j}(t). \tag{5.58}$$
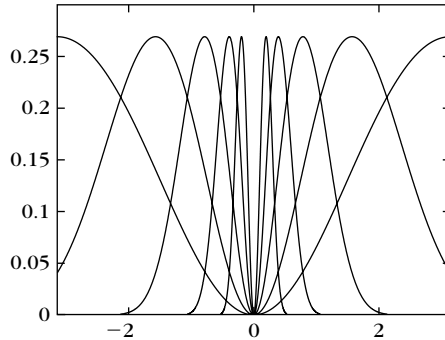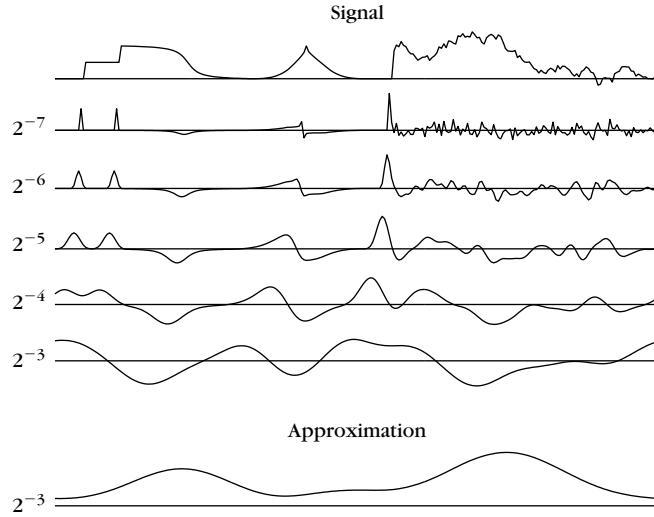

FIGURE 5.1

Scaled Fourier transforms $|\hat{\psi}(2^j\omega)|^2$ computed with (5.69), for $1 \leq j \leq 5$ and $\omega \in [-\pi, \pi]$.

FIGURE 5.2

Dyadic wavelet transform $Wf(u, 2^j)$ computed at scales $2^{-7} \leqslant 2^j \leqslant 2^{-3}$ with filter bank algorithm from Section 5.2.2, for a signal defined over $[0, 1]$. The bottom curve carries lower frequencies corresponding to scales larger than 2^{-3}.

Figure 5.2 gives a dyadic wavelet transform computed over five scales with the quadratic spline wavelet shown later in Figure 5.3.

5.2.1 Dyadic Wavelet Design

A discrete dyadic wavelet transform can be computed with a fast filter bank algorithm if the wavelet is appropriately designed. The synthesis of these dyadic wavelets is similar to the construction of biorthogonal wavelet bases, explained in Section 7.4. All technical issues related to the convergence of infinite cascades of filters are avoided in this section. Reading Chapter 7 first is necessary for understanding the main results.

Let h and g be a pair of finite impulse-response filters. Suppose that h is a low-pass filter with a transfer function that satisfies $\hat{h}(0) = \sqrt{2}$. As in the case of orthogonal and biorthogonal wavelet bases, we construct a scaling function with a Fourier transform:

$$\hat{\phi}(\omega) = \prod_{p=1}^{+\infty} \frac{\hat{h}(2^{-p}\omega)}{\sqrt{2}} = \frac{1}{\sqrt{2}} \hat{h}\left(\frac{\omega}{2}\right)\hat{\phi}\left(\frac{\omega}{2}\right). \tag{5.59}$$

We suppose here that this Fourier transform is a finite-energy function so that $\phi \in \mathbf{L}^2(\mathbb{R})$. The corresponding wavelet ψ has a Fourier transform defined by

$$\hat{\psi}(\omega) = \frac{1}{\sqrt{2}} \hat{g}\left(\frac{\omega}{2}\right) \hat{\phi}\left(\frac{\omega}{2}\right). \tag{5.60}$$

Theorem 7.5 proves that both ϕ and ψ have a compact support because h and g have a finite number of nonzero coefficients. The number of vanishing moments of ψ is equal to the number of zeroes of $\hat{\psi}(\omega)$ at $\omega = 0$. Since $\hat{\phi}(0) = 1$, (5.60) implies that it is also equal to the number of zeros of $\hat{g}(\omega)$ at $\omega = 0$.

Reconstructing Wavelets

Reconstructing wavelets that satisfy (5.49) are calculated with a pair of finite impulse response dual filters $\tilde{h}$ and $\tilde{g}$. We suppose that the following Fourier transform has a finite energy:

$$\widehat{\tilde{\phi}}(\omega) = \prod_{p=1}^{+\infty} \frac{\widehat{\tilde{h}}(2^{-p}\omega)}{\sqrt{2}} = \frac{1}{\sqrt{2}} \widehat{\tilde{h}}\left(\frac{\omega}{2}\right) \widehat{\tilde{\phi}}\left(\frac{\omega}{2}\right). \qquad (5.61)$$

Let us define

$$\widehat{\tilde{\psi}}(\omega) = \frac{1}{\sqrt{2}} \widehat{\tilde{g}}\left(\frac{\omega}{2}\right) \widehat{\tilde{\phi}}\left(\frac{\omega}{2}\right). \qquad (5.62)$$

Theorem 5.13 gives a sufficient condition to guarantee that $\widehat{\tilde{\psi}}$ is the Fourier transform of a reconstruction wavelet.

Theorem 5.13. If the filters satisfy

$$\forall \omega \in [-\pi, \pi], \quad \widehat{\tilde{h}}(\omega)\,\hat{h}^*(\omega) + \widehat{\tilde{g}}(\omega)\,\hat{g}^*(\omega) = 2, \qquad (5.63)$$

then

$$\forall \omega \in \mathbb{R} - \{0\}, \quad \sum_{j=-\infty}^{+\infty} \hat{\psi}^*(2^j\omega)\,\widehat{\tilde{\psi}}(2^j\omega) = 1. \qquad (5.64)$$

Proof. The Fourier transform expressions (5.60) and (5.62) prove that

$$\widehat{\tilde{\psi}}(\omega)\,\hat{\psi}^*(\omega) = \frac{1}{2} \widehat{\tilde{g}}\left(\frac{\omega}{2}\right) \hat{g}^*\left(\frac{\omega}{2}\right) \widehat{\tilde{\phi}}\left(\frac{\omega}{2}\right) \hat{\phi}^*\left(\frac{\omega}{2}\right).$$

Equation (5.63) implies

$$\widehat{\tilde{\psi}}(\omega)\,\hat{\psi}^*(\omega) = \frac{1}{2} \left[2 - \widehat{\tilde{h}}\left(\frac{\omega}{2}\right) \hat{h}^*\left(\frac{\omega}{2}\right)\right] \widehat{\tilde{\phi}}\left(\frac{\omega}{2}\right) \hat{\phi}^*\left(\frac{\omega}{2}\right)$$

$$= \widehat{\tilde{\phi}}\left(\frac{\omega}{2}\right) \hat{\phi}^*\left(\frac{\omega}{2}\right) - \widehat{\tilde{\phi}}(\omega)\,\hat{\phi}^*(\omega).$$

Therefore,

$$\sum_{j=-l}^{k} \widehat{\tilde{\psi}}(2^j\omega)\,\hat{\psi}^*(2^j\omega) = \hat{\phi}^*(2^{-l}\omega)\,\widehat{\tilde{\phi}}(2^{-l}\omega) - \hat{\phi}^*(2^k\omega)\,\widehat{\tilde{\phi}}(2^k\omega).$$

Since $\hat{g}(0) = 0$, (5.63) implies $\widehat{\tilde{h}}(0)\,\hat{h}^*(0) = 2$. We also impose that $\hat{h}(0) = \sqrt{2}$, so one can derive from (5.59) and (5.61) that $\widehat{\tilde{\phi}}(0) = \hat{\phi}^*(0) = 1$. Since ϕ and $\tilde{\phi}$ belong to $\mathbf{L}^1(\mathbb{R})$,

$\hat{\phi}$ and $\hat{\tilde{\phi}}$ are continuous, and the Riemann-Lebesgue lemma (Exercise 2.8) proves that $|\hat{\phi}(\omega)|$ and $|\hat{\tilde{\phi}}(\omega)|$ decrease to zero when ω goes to ∞. For $\omega \neq 0$, letting k and l go to $+\infty$ yields (5.64). ∎

Observe that (5.63) is the same as the unit gain condition (7.117) for biorthogonal wavelets. The aliasing cancellation condition (7.116) of biorthogonal wavelets is not required because the wavelet transform is not sampled in time.

Finite Impulse Response Solution

Let us shift h and g to obtain causal filters. The resulting transfer functions $\hat{h}(\omega)$ and $\hat{g}(\omega)$ are polynomials in $e^{-i\omega}$. We suppose that these polynomials have no common zeros. The Bezout theorem (7.8) on polynomials proves that if $P(z)$ and $Q(z)$ are two polynomials of degree n and l, with no common zeros, then there exists a unique pair of polynomials $\tilde{P}(z)$ and $\tilde{Q}(z)$ of degree $l - 1$ and $n - 1$ such that

$$P(z)\,\tilde{P}(z) + Q(z)\,\tilde{Q}(z) = 1. \tag{5.65}$$

This guarantees the existence of $\hat{\tilde{h}}(\omega)$ and $\hat{\tilde{g}}(\omega)$, which are polynomials in $e^{-i\omega}$ and satisfy (5.63). These are the Fourier transforms of the finite impulse response filters $\tilde{h}$ and $\tilde{g}$. However, one must be careful, because the resulting scaling function $\hat{\tilde{\phi}}$ in (5.61) does not necessarily have a finite energy.

Spline Dyadic Wavelets

A *box spline* of degree m is a translation of $m + 1$ convolutions of $\mathbf{1}_{[0,1]}$ with itself. It is centered at $t = 1/2$ if m is even and at $t = 0$ if m is odd. Its Fourier transform is

$$\hat{\phi}(\omega) = \left(\frac{\sin(\omega/2)}{\omega/2}\right)^{m+1} \exp\left(\frac{-i\varepsilon\omega}{2}\right) \quad \text{with} \quad \varepsilon = \begin{cases} 1 & \text{if } m \text{ is even} \\ 0 & \text{if } m \text{ is odd} \end{cases}, \tag{5.66}$$

so

$$\hat{h}(\omega) = \sqrt{2}\,\frac{\hat{\phi}(2\omega)}{\hat{\phi}(\omega)} = \sqrt{2}\,\left(\cos\frac{\omega}{2}\right)^{m+1} \exp\left(\frac{-i\varepsilon\omega}{2}\right). \tag{5.67}$$
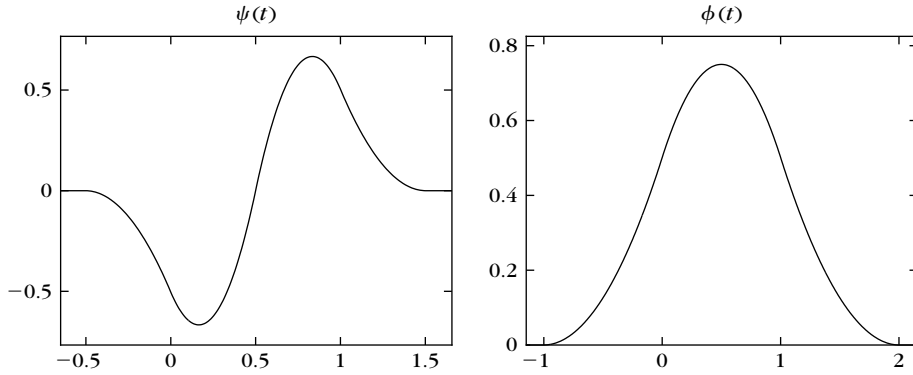
We construct a wavelet that has one vanishing moment by choosing $\hat{g}(\omega) = O(\omega)$ in the neighborhood of $\omega = 0$. For example,

$$\hat{g}(\omega) = -i\,\sqrt{2}\,\sin\frac{\omega}{2}\,\exp\left(\frac{-i\varepsilon\omega}{2}\right). \tag{5.68}$$

The Fourier transform of the resulting wavelet is

$$\hat{\psi}(\omega) = \frac{1}{\sqrt{2}}\,\hat{g}\left(\frac{\omega}{2}\right)\hat{\phi}\left(\frac{\omega}{2}\right) = \frac{-i\omega}{4}\,\left(\frac{\sin(\omega/4)}{\omega/4}\right)^{m+2} \exp\left(\frac{-i\omega(1+\varepsilon)}{4}\right). \tag{5.69}$$

It is the first derivative of a box spline of degree $m + 1$ centered at $t = (1 + \varepsilon)/4$. For $m = 2$, Figure 5.3 shows the resulting quadratic splines ϕ and ψ. The

FIGURE 5.3

Quadratic spline wavelet and scaling function.

Table 5.1 Coefficients of Filters Computed from the Transfer Functions (5.67, 5.68, 5.70) for $m = 2$

n	$h[n]/\sqrt{2}$	$\tilde{h}[n]/\sqrt{2}$	$g[n]/\sqrt{2}$	$\tilde{g}[n]/\sqrt{2}$
-2				-0.03125
-1	0.125	0.125		-0.21875
0	0.375	0.375	-0.5	-0.6875
1	0.375	0.375	0.5	0.6875
2	0.125	0.125		0.21875
3				0.03125

Note: These filters generate the quadratic spline scaling functions and wavelets shown in Figure 5.3.

dyadic admissibility condition (5.48) is verified numerically for $A = 0.505$ and $B = 0.522$.

To design dual-scaling functions $\tilde{\phi}$ and wavelets $\tilde{\psi}$ that are splines, we choose $\widehat{\tilde{h}} = \hat{h}$. As a consequence, $\phi = \tilde{\phi}$ and the reconstruction condition (5.63) imply that

$$\widehat{\tilde{g}}(\omega) = \frac{2 - |\hat{h}(\omega)|^2}{\hat{g}^*(\omega)} = -i\sqrt{2}\,\exp\left(\frac{-i\omega}{2}\right)\sin\frac{\omega}{2}\sum_{n=0}^{m}\left(\cos\frac{\omega}{2}\right)^{2n}. \qquad (5.70)$$

Table 5.1 gives the corresponding filters for $m = 2$.

5.2.2 Algorithme à Trous

Suppose that the scaling functions and wavelets $\phi, \psi, \tilde{\phi}$, and $\tilde{\psi}$ are designed with the filters $h, g, \tilde{h}$, and $\tilde{g}$. A fast dyadic wavelet transform is calculated with a filter bank

algorithm, called *algorithme à trous*, introduced by Holschneider et al. [303]. It is similar to a fast biorthogonal wavelet transform, without subsampling [367, 433].

Fast Dyadic Transform

The samples $a_0[n]$ of the input discrete signal are written as a low-pass filtering with ϕ of an analog signal f, in the neighborhood of $t = n$:

$$a_0[n] = f \star \bar{\phi}(n) = \langle f(t), \phi(t - n) \rangle = \int_{-\infty}^{+\infty} f(t)\, \phi(t - n)\, dt.$$

This is further justified in Section 7.3.1. For any $j \geqslant 0$, we denote

$$a_j[n] = \langle f(t), \phi_{2^j}(t - n) \rangle \quad \text{with} \quad \phi_{2^j}(t) = \frac{1}{\sqrt{2^j}} \phi\left(\frac{t}{2^j}\right).$$

The dyadic wavelet coefficients are computed for $j > 0$ over the integer grid

$$d_j[n] = Wf(n, 2^j) = \langle f(t), \psi_{2^j}(t - n) \rangle.$$

For any filter $x[n]$, we denote by $x_j[n]$ the filters obtained by inserting $2^j - 1$ zeros between each sample of $x[n]$. Its Fourier transform is $\hat{x}(2^j \omega)$. Inserting zeros in the filters creates holes (*trous* in French). Let $\bar{x}_j[n] = x_j[-n]$. Theorem 5.14 gives convolution formulas that are cascaded to compute a dyadic wavelet transform and its inverse.

Theorem 5.14. For any $j \geqslant 0$,

$$a_{j+1}[n] = a_j \star \bar{h}_j[n], \quad d_{j+1}[n] = a_j \star \bar{g}_j[n], \tag{5.71}$$

and

$$a_j[n] = \frac{1}{2}\left(a_{j+1} \star \tilde{h}_j[n] + d_{j+1} \star \tilde{g}_j[n]\right). \tag{5.72}$$

Proof of (5.71). Since

$$a_{j+1}[n] = f \star \bar{\phi}_{2^{j+1}}(n) \quad \text{and} \quad d_{j+1}[n] = f \star \bar{\psi}_{2^{j+1}}(n),$$

we verify with (3.3) that their Fourier transforms are, respectively,

$$\hat{a}_{j+1}(\omega) = \sum_{k=-\infty}^{+\infty} \hat{f}(\omega + 2k\pi)\, \hat{\phi}_{2^{j+1}}^*(\omega + 2k\pi)$$

and

$$\hat{d}_{j+1}(\omega) = \sum_{k=-\infty}^{+\infty} \hat{f}(\omega + 2k\pi)\, \hat{\psi}_{2^{j+1}}^*(\omega + 2k\pi).$$

The properties (5.61) and (5.62) imply that

$$\hat{\phi}_{2^{j+1}}(\omega) = \sqrt{2^{j+1}}\, \hat{\phi}(2^{j+1}\omega) = \hat{h}(2^j \omega)\, \sqrt{2^j}\, \hat{\phi}(2^j \omega),$$
$$\hat{\psi}_{2^{j+1}}(\omega) = \sqrt{2^{j+1}}\, \hat{\psi}(2^{j+1}\omega) = \hat{g}(2^j \omega)\, \sqrt{2^j}\, \hat{\phi}(2^j \omega).$$

Since $j \geqslant 0$, both $\hat{h}(2^j\omega)$ and $\hat{g}(2^j\omega)$ are 2π periodic, so

$$\hat{a}_{j+1}(\omega) = \hat{h}^*(2^j\omega)\,\hat{a}_j(\omega) \quad \text{and} \quad \hat{d}_{j+1}(\omega) = \hat{g}^*(2^j\omega)\,\hat{a}_j(\omega). \tag{5.73}$$

These two equations are the Fourier transforms of (5.71).

Proof of (5.72). Equation (5.73) implies

$$\hat{a}_{j+1}(\omega)\,\widehat{\overline{h}}(2^j\omega) + \hat{d}_{j+1}(\omega)\,\widehat{\overline{g}}(2^j\omega) =$$

$$\hat{a}_j(\omega)\,\hat{h}^*(2^j\omega)\,\widehat{\overline{h}}(2^j\omega) + \hat{a}_j(\omega)\,\hat{g}^*(2^j\omega)\,\widehat{\overline{g}}(2^j\omega).$$

Inserting the reconstruction condition (5.63) proves that

$$\hat{a}_{j+1}(\omega)\,\widehat{\overline{h}}(2^j\omega) + \hat{d}_{j+1}(\omega)\,\widehat{\overline{g}}(2^j\omega) = 2\,\hat{a}_j(\omega),$$

which is the Fourier transform of (5.72). ∎

The dyadic wavelet representation of a_0 is defined as the set of wavelet coefficients up to a scale 2^J plus the remaining low-frequency information a_J:

$$\left[\{d_j\}_{1 \leqslant j \leqslant J}, \ a_J\right]. \tag{5.74}$$

It is computed from a_0 by cascading the convolutions (5.71) for $0 \leqslant j < J$, as illustrated in Figure 5.4(a). The dyadic wavelet transform of Figure 5.2 is calculated with the filter bank algorithm. The original signal a_0 is recovered from its wavelet representation (5.74) by iterating (5.72) for $J > j \geqslant 0$, as illustrated in Figure 5.4(b).

If the input signal $a_0[n]$ has a finite size of N samples, the convolutions (5.71) are replaced by circular convolutions. The maximum scale 2^J is then limited to N, and for $J = \log_2 N$, one can verify that $a_J[n]$ is constant and equal to $N^{-1/2}\sum_{n=0}^{N-1} a_0[n]$. Suppose that h and g have, respectively, K_h and K_g nonzero samples. The "dilated" filters h_j and g_j have the same number of nonzero coefficients. Therefore, the number of multiplications needed to compute a_{j+1} and d_{j+1} from a_j or the reverse
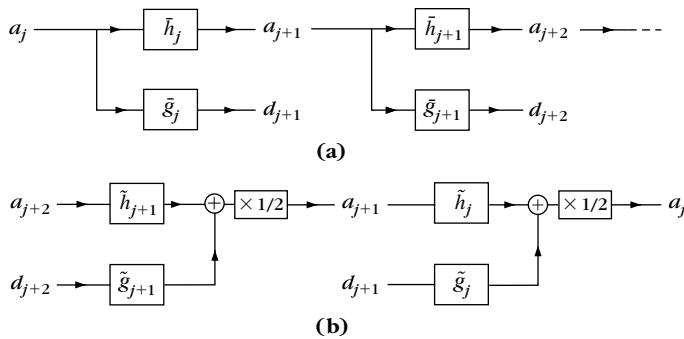

(a)

(b)

FIGURE 5.4

(a) The dyadic wavelet coefficients are computed by cascading convolutions with dilated filters $\bar{h}_j$ and $\bar{g}_j$. **(b)** The original signal is reconstructed through convolutions with $\tilde{h}_j$ and $\tilde{g}_j$. A multiplication by $1/2$ is necessary to recover the next finer scale signal a_j.

is equal to $(K_h + K_g)N$. Thus, for $J = \log_2 N$, the dyadic wavelet representation (5.74) and its inverse are calculated with $(K_h + K_g)N \log_2 N$ multiplications and additions.

5.3 SUBSAMPLED WAVELET FRAMES

Wavelet frames are constructed by sampling the scale parameter but also the translation parameter of a wavelet dictionary. A real continuous wavelet transform of $f \in \mathbf{L}^2(\mathbb{R})$ is defined in Section 4.3 by

$$W f(u, s) = \langle f, \psi_{u,s} \rangle \quad \text{with} \quad \psi_{u,s}(t) = \frac{1}{\sqrt{s}} \psi\left(\frac{t-u}{s}\right),$$

where ψ is a real wavelet. Imposing $\|\psi\| = 1$ implies that $\|\psi_{u,s}\| = 1$.

Intuitively, to construct a frame we need to cover the time-frequency plane with the Heisenberg boxes of the corresponding discrete wavelet family. A wavelet $\psi_{u,s}$ has an energy in time that is centered at u over a domain proportional to s. For positive frequencies, its Fourier transform $\hat{\psi}_{u,s}$ has a support centered at a frequency η/s, with a spread proportional to $1/s$. To obtain a full cover, we sample s along an exponential sequence $\{a^j\}_{j\in\mathbb{Z}}$, with a sufficiently small dilation step $a > 1$. The time translation u is sampled uniformly at intervals proportional to the scale a^j, as illustrated in Figure 5.5. Let us denote

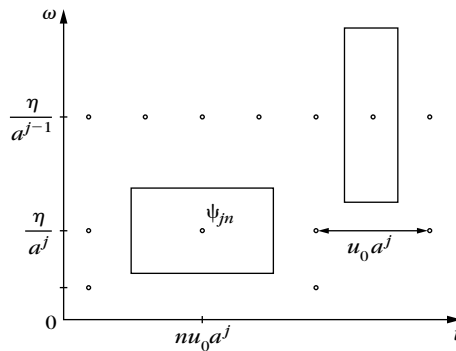$$\psi_{j,n}(t) = \frac{1}{\sqrt{a^j}} \psi\left(\frac{t - nu_0 a^j}{a^j}\right).$$

FIGURE 5.5

The Heisenberg box of a wavelet $\psi_{j,n}$ scaled by $s = a^j$ has a time and frequency width proportional to a^j and a^{-j}, respectively. The time-frequency plane is covered by these boxes if u_0 and a are sufficiently small.

In the following, we give without proof, some necessary conditions and sufficient conditions on ψ, a and u_0 so that $\{\psi_{j,n}\}_{(j,n)\in\mathbb{Z}^2}$ is a frame of $\mathbf{L}^2(\mathbb{R})$.

Necessary Conditions

We suppose that ψ is real, normalized, and satisfies the admissibility condition of Theorem 4.4:

$$C_\psi = \int_0^{+\infty} \frac{|\hat{\psi}(\omega)|^2}{\omega} \, d\omega < +\infty. \tag{5.75}$$

Theorem 5.15: *Daubechies.* If $\{\psi_{j,n}\}_{(j,n)\in\mathbb{Z}^2}$ is a frame of $\mathbf{L}^2(\mathbb{R})$, then the frame bounds satisfy

$$A \leqslant \frac{C_\psi}{u_0 \, \log_e a} \leqslant B, \tag{5.76}$$

$$\forall \omega \in \mathbb{R} - \{0\}, \quad A \leqslant \frac{1}{u_0} \sum_{j=-\infty}^{+\infty} |\hat{\psi}(a^j\omega)|^2 \leqslant B. \tag{5.77}$$

This theorem is proved in [19, 163]. Condition (5.77) is equivalent to the frame condition (5.55) for a translation-invariant dyadic wavelet transform, for which the parameter u is not sampled. It requires that the Fourier axis is covered by wavelets dilated by $\{a^j\}_{j\in\mathbb{Z}}$. The inequality (5.76), which relates the sampling density $u_0 \log_e a$ to the frame bounds, is proved in [19]. It shows that the frame is an orthonormal basis if and only if

$$A = B = \frac{C_\psi}{u_0 \, \log_e a} = 1.$$

Chapter 7 constructs wavelet orthonormal bases of $\mathbf{L}^2(\mathbb{R})$ with regular wavelets of compact support.

Sufficient Conditions

Theorem 5.16 proved by Daubechies [19] provides a lower and upper bound for the frame bounds A and B, depending on ψ, u_0, and a.

Theorem 5.16: *Daubechies.* Let us define

$$\theta(\xi) = \sup_{1 \leqslant |\omega| \leqslant a} \sum_{j=-\infty}^{+\infty} |\hat{\psi}(a^j\omega)| \, |\hat{\psi}(a^j\omega + \xi)| \tag{5.78}$$

and

$$\Delta = \sum_{\substack{k=-\infty \\ k\neq 0}}^{+\infty} \left[\theta\left(\frac{2\pi k}{u_0}\right) \theta\left(\frac{-2\pi k}{u_0}\right) \right]^{1/2}.$$

If u_0 and a are such that

$$A_0 = \frac{1}{u_0}\left(\inf_{1\leqslant|\omega|\leqslant a}\sum_{j=-\infty}^{+\infty}|\hat{\psi}(a^j\omega)|^2 - \Delta\right) > 0, \tag{5.79}$$

and

$$B_0 = \frac{1}{u_0}\left(\sup_{1\leqslant|\omega|\leqslant a}\sum_{j=-\infty}^{+\infty}|\hat{\psi}(a^j\omega)|^2 + \Delta\right) < +\infty, \tag{5.80}$$

then $\{\psi_{j,n}\}_{(j,n)\in\mathbb{Z}^2}$ is a frame of $\mathbf{L}^2(\mathbb{R})$. The constants A_0 and B_0 are respectively lower and upper bounds of the frame bounds A and B.

The sufficient conditions (5.79) and (5.80) are similar to the necessary condition (5.77). If Δ is small relative to $\inf_{1\leqslant|\omega|\leqslant a}\sum_{j=-\infty}^{+\infty}|\hat{\psi}(a^j\omega)|^2$, then A_0 and B_0 are close to the optimal frame bounds A and B. For a fixed dilation step a, the value of Δ decreases when the time-sampling interval u_0 decreases.

Dual Frame
Theorem 5.5 gives a general formula for computing the dual-wavelet frame vectors

$$\tilde{\psi}_{j,n} = (\Phi^*\Phi)^{-1}\psi_{j,n}. \tag{5.81}$$

One could reasonably hope that the dual functions $\tilde{\psi}_{j,n}$ would be obtained by scaling and translating a dual wavelet $\tilde{\psi}$. The unfortunate reality is that this is generally not true. In general, the operator $\Phi^*\Phi$ does not commute with dilations by a^j, so $(\Phi^*\Phi)^{-1}$ does not commute with these dilations either. On the other hand, one can prove that $(\Phi^*\Phi)^{-1}$ commutes with translations by na^ju_0, which means that

$$\tilde{\psi}_{j,n}(t) = \tilde{\psi}_{j,0}(t - na^ju_0). \tag{5.82}$$

Thus, the dual frame $\{\tilde{\psi}_{j,n}\}_{(j,n)\in\mathbb{Z}^2}$ is obtained by calculating each elementary function $\tilde{\psi}_{j,0}$ with (5.81), and translating them with (5.82). The situation is much simpler for tight frames, where the dual frame is equal to the original wavelet frame.

Mexican Hat Wavelet
The normalized second derivative of a Gaussian is

$$\psi(t) = \frac{2}{\sqrt{3}}\,\pi^{-1/4}\,(t^2-1)\,\exp\left(\frac{-t^2}{2}\right). \tag{5.83}$$

Its Fourier transform is

$$\hat{\psi}(\omega) = -\frac{\sqrt{8}\,\pi^{1/4}\,\omega^2}{\sqrt{3}}\,\exp\left(\frac{-\omega^2}{2}\right).$$

The graph of these functions is shown in Figure 4.6.

a	u_0	A_0	B_0	B_0/A_0
Table 5.2 Estimated Frame Bounds for the Mexican Hat Wavelet				
2	0.25	13.091	14.183	1.083
2	0.5	6.546	7.092	1.083
2	1.0	3.223	3.596	1.116
2	1.5	0.325	4.221	12.986
$2^{\frac{1}{2}}$	0.25	27.273	27.278	1.0002
$2^{\frac{1}{2}}$	0.5	13.673	13.639	1.0002
$2^{\frac{1}{2}}$	1.0	6.768	6.870	1.015
$2^{\frac{1}{2}}$	1.75	0.517	7.276	14.061
$2^{\frac{1}{4}}$	0.25	54.552	54.552	1.0000
$2^{\frac{1}{4}}$	0.5	27.276	27.276	1.0000
$2^{\frac{1}{4}}$	1.0	13.586	13.690	1.007
$2^{\frac{1}{4}}$	1.75	2.928	12.659	4.324
Source: Computed with Theorem 5.16 [19].				

The dilation step a is generally set to be $a = 2^{1/v}$ where v is the number of intermediate scales (voices) for each octave. Table 5.2 gives the estimated frame bounds A_0 and B_0 computed by Daubechies [19] with the formula of Theorem 5.16. For $v \geqslant 2$ voices per octave, the frame is nearly tight when $u_0 \leqslant 0.5$, in which case the dual frame can be approximated by the original wavelet frame. As expected from (5.76), when $A \approx B$,

$$A \approx B \approx \frac{C_\psi}{u_0 \log_e a} = \frac{v}{u_0} C_\psi \log_2 e.$$

The frame bounds increase proportionally to v/u_0. For $a = 2$, we see that A_0 decreases brutally from $u_0 = 1$ to $u_0 = 1.5$. For $u_0 = 1.75$, the wavelet family is not a frame anymore. For $a = 2^{1/2}$, the same transition appears for a larger u_0.

5.4 WINDOWED FOURIER FRAMES

Frame theory gives conditions for discretizing the windowed Fourier transform while retaining a complete and stable representation. The windowed Fourier transform of $f \in \mathbf{L}^2(\mathbb{R})$ is defined in Section 4.2 by

$$Sf(u, \xi) = \langle f, g_{u,\xi} \rangle,$$

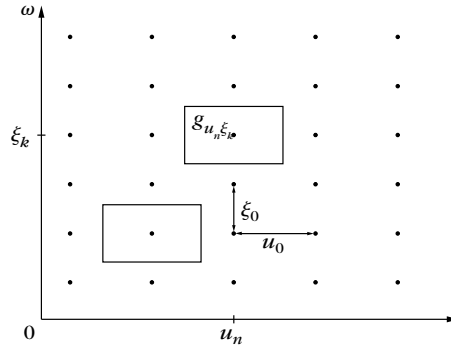with

$$g_{u,\xi}(t) = g(t - u)\, e^{i\xi t}.$$

FIGURE 5.6

A windowed Fourier frame is obtained by covering the time-frequency plane with a regular grid of windowed Fourier atoms, translated by $u_n = n\,u_0$ in time and by $\xi_k = k\,\xi_0$ in frequency.

Setting $\|g\| = 1$ implies that $\|g_{u,\xi}\| = 1$. A discrete windowed Fourier transform representation

$$\{Sf(u_n, \xi_k) = \langle f, g_{u_n,\xi_k}\rangle\}_{(n,k)\in\mathbb{Z}^2}$$

is complete and stable if $\{g_{u,n,\xi_k}\}_{(n,k)\in\mathbb{Z}^2}$ is a frame of $\mathbf{L}^2(\mathbb{R})$.

Intuitively, one can expect that the discrete windowed Fourier transform is complete if the Heisenberg boxes of all atoms $\{g_{u,n,\xi_k}\}_{(n,k)\in\mathbb{Z}^2}$ fully cover the time-frequency plane. Section 4.2 shows that the Heisenberg box of g_{u_n,ξ_k} is centered in the time-frequency plane at (u_n, ξ_k). Its size is independent of u_n and ξ_k. It depends on the time-frequency spread of the window g. Thus, a complete cover of the plane is obtained by translating these boxes over a uniform rectangular grid, as illustrated in Figure 5.6. The time and frequency parameters (u, ξ) are discretized over a rectangular grid with time and frequency intervals of size u_0 and ξ_0. Let us denote

$$g_{n,k}(t) = g(t - nu_0)\,\exp(ik\xi_0 t).$$

The sampling intervals (u_0, ξ_0) must be adjusted to the time-frequency spread of g.

Window Scaling

Suppose that $\{g_{n,k}\}_{(n,k)\in\mathbb{Z}^2}$ is a frame of $\mathbf{L}^2(\mathbb{R})$ with frame bounds A and B. Let us dilate the window $g_s(t) = s^{-1/2}g(t/s)$. It increases by s the time width of the Heisenberg box of g and reduces by s its frequency width. Thus, we obtain the same cover of the time-frequency plane by increasing u_0 by s and reducing ξ_0 by s. Let

$$g_{s,n,k}(t) = g_s(t - nsu_0)\,\exp\left(ik\frac{\xi_0}{s}t\right). \tag{5.84}$$

We prove that $\{g_{s,n,k}\}_{(n,k)\in\mathbb{Z}^2}$ satisfies the same frame inequalities as $\{g_{n,k}\}_{(n,k)\in\mathbb{Z}^2}$, with the same frame bounds A and B, by a change of variable $t' = ts$ in the inner product integrals.

5.4.1 Tight Frames

Tight frames are easier to manipulate numerically since the dual frame is equal to the original frame. Daubechies, Grossmann, and Meyer [197] give sufficient conditions for building a window of compact support that generates a tight frame.

Theorem 5.17: *Daubechies, Grossmann, Meyer.* Let g be a window that has a support included in $[-\pi/\xi_0, \pi/\xi_0]$. If

$$\forall t \in \mathbb{R}, \quad \frac{2\pi}{\xi_0} \sum_{n=-\infty}^{+\infty} |g(t - nu_0)|^2 = A > 0, \tag{5.85}$$

then $\{g_{n,k}(t) = g(t - nu_0)\,e^{ik\xi_0 t}\}_{(n,k)\in\mathbb{Z}^2}$ is a tight frame $\mathbf{L}^2(\mathbb{R})$ with a frame bound equal to A.

Proof. The function $g(t - nu_0)f(t)$ has a support in $[nu_0 - \pi/\xi_0, nu_0 + \pi/\xi_0]$. Since $\{e^{ik\xi_0 t}\}_{k\in\mathbb{Z}}$ is an orthogonal basis of this space, we have

$$\int_{-\infty}^{+\infty} |g(t - nu_0)|^2 \, |f(t)|^2 dt = \int_{nu_0 - \pi/\xi_0}^{nu_0 + \pi/\xi_0} |g(t - nu_0)|^2 \, |f(t)|^2 dt$$

$$= \frac{\xi_0}{2\pi} \sum_{k=-\infty}^{+\infty} |\langle g(u - nu_0)f(u), e^{ik\xi_0 u}\rangle|^2.$$

Since $g_{n,k}(t) = g(t - nu_0)\,e^{ik\xi_0 t}$, we get

$$\int_{-\infty}^{+\infty} |g(t - nu_0)|^2 \, |f(t)|^2 dt = \frac{\xi_0}{2\pi} \sum_{k=-\infty}^{+\infty} |\langle f, g_{n,k}\rangle|^2.$$

Summing over n and inserting (5.85) proves that $A \|f\|^2 = \sum_{k,n=-\infty}^{+\infty} |\langle f, g_{n,k}\rangle|^2$, and therefore, that $\{g_{n,k}\}_{(n,k)\in\mathbb{Z}^2}$ is a tight frame of $\mathbf{L}^2(\mathbb{R})$. ∎

Since g has a support in $[-\pi/\xi_0, \pi/\xi_0]$ the condition (5.85) implies that

$$\frac{2\pi}{u_0 \xi_0} \geqslant 1,$$

so that there is no whole between consecutive windows $g(t - nu_0)$ and $g(t - (n + 1)u_0)$. If we impose that $1 \leqslant 2\pi/(u_0\xi_0) \leqslant 2$, then only consecutive windows have supports that overlap. The square root of a Hanning window

$$g(t) = \sqrt{\frac{\xi_0}{\pi}} \, \cos\left(\frac{\xi_0 t}{2}\right) \mathbf{1}_{[-\pi/\xi_0, \pi/\xi_0]}(t)$$

is a positive normalized window that satisfies (5.85) with $u_0 = \pi/\xi_0$ and a redundancy factor of $A = 2$. The design of other windows is studied in Section 8.4.2 for local cosine bases.

Discrete Window Fourier Tight Frames

To construct a windowed Fourier tight frame of $\mathbb{C}^N$, the Fourier basis $\{e^{ik\xi_0 t}\}_{k\in\mathbb{Z}}$ of $\mathbf{L}^2[-\pi/\xi_0, \pi/\xi_0]$ is replaced by the discrete Fourier basis $\{e^{i2\pi kn/K}\}_{0\leq k<K}$ of $\mathbb{C}^K$. Theorem 5.18 is a discrete equivalent of Theorem 5.17.

Theorem 5.18. Let $g[n]$ be an N periodic discrete window with a support and restricted to $[-N/2, N/2]$ that is included in $[-K/2, K/2-1]$. If M divides N and

$$\forall 0 \leq n < N, \quad K \sum_{m=0}^{N/M-1} |g[n-mM]|^2 = A > 0, \tag{5.86}$$

then $\{g_{m,k}[n] = g[n-mM]\,e^{i2\pi kn/K}\}_{0\leq k<K, 0\leq m<N/M}$ is a tight frame $\mathbb{C}^N$ with a frame bound equal to A.

The proof of this theorem follows the same steps as the proof of Theorem 5.17. It is left in Exercise 5.10. There are N/M translated windows and thus NK/M windowed Fourier coefficients. For a fixed window position indexed by m, the discrete windowed Fourier coefficients are the discrete Fourier coefficients of the windowed signal

$$Sf[m, k] = \langle f, g_{m,k}\rangle = \sum_{n=K/2}^{K/2-1} f[n]\,g[n-mM]\,e^{-i2\pi kn/K} \quad \text{for} \quad 0 \leq k < K.$$

They are computed with $O(K \log_2 K)$ operations with an FFT. Over all windows, this requires a total of $O(NK/M \log_2 K)$ operations. We generally choose $1 < K/M \leq 2$ so that only consecutive windows overlap. The square root of a Hanning window $g[n] = \sqrt{2/K}\,\cos(\pi n/K)$ satisfies (5.86) for $M = K/2$ and a redundancy factor $A = 2$. Figure 5.7 shows the log spectrogram $\log|Sf[m, k]|^2$ of the windowed Fourier frame coefficients computed with a square root Hanning window for a musical recording.

5.4.2 General Frames

For general windowed Fourier frames of $\mathbf{L}^2(\mathbb{R}^2)$, Daubechies [19] proved several necessary conditions on g, u_0 and ξ_0 to guarantee that $\{g_{n,k}\}_{(n,k)\in\mathbb{Z}^2}$ is a frame of $\mathbf{L}^2(\mathbb{R})$. We do not reproduce the proofs, but summarize the main results.

Theorem 5.19: *Daubechies*. The windowed Fourier family $\{g_{n,k}\}_{(n,k)\in\mathbb{Z}^2}$ is a frame only if

$$\frac{2\pi}{u_0\,\xi_0} \geq 1. \tag{5.87}$$

The frame bounds A and B necessarily satisfy

$$A \leq \frac{2\pi}{u_0\,\xi_0} \leq B, \tag{5.88}$$

(a)

(b)
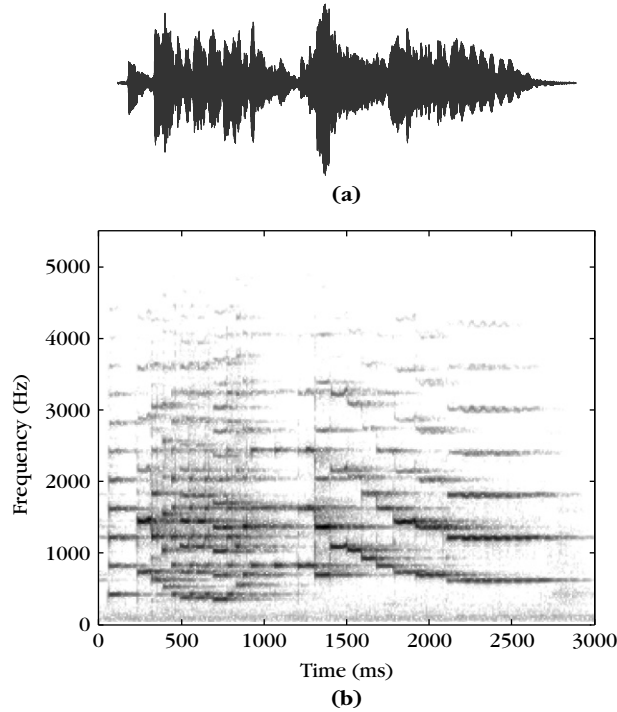
FIGURE 5.7

(a) Musical recording. (b) Log spectrogram $\log |Sf[m, k]|^2$ computed with a square root Hanning window.

$$\forall t \in \mathbb{R}, \quad A \leqslant \frac{2\pi}{\xi_0} \sum_{n=-\infty}^{+\infty} |g(t - nu_0)|^2 \leqslant B, \tag{5.89}$$

$$\forall \omega \in \mathbb{R}, \quad A \leqslant \frac{1}{u_0} \sum_{k=-\infty}^{+\infty} |\hat{g}(\omega - k\xi_0)|^2 \leqslant B. \tag{5.90}$$

The ratio $2\pi/(u_0\xi_0)$ measures the density of windowed Fourier atoms in the time-frequency plane. The first condition (5.87) ensures that this density is greater than 1 because the covering ability of each atom is limited. Inequalities (5.89) and (5.90) are proved in full generality by Chui and Shi [163]. They show that the uniform time translations of g must completely cover the time axis, and the frequency translations of its Fourier transform $\hat{g}$ must similarly cover the frequency axis.

Since all windowed Fourier vectors are normalized, the frame is an orthogonal basis only if $A = B = 1$. The frame bound condition (5.88) shows that this is possible only at the critical sampling density $u_0\xi_0 = 2\pi$. The Balian-Low theorem 5.20 [93] proves that g is then either nonsmooth or has a slow time decay.

Theorem 5.20: *Balian-Low.* If $\{g_{n,k}\}_{(n,k)\in\mathbb{Z}^2}$ is a windowed Fourier frame with $u_0\xi_0 = 2\pi$, then

$$\int_{-\infty}^{+\infty} t^2 |g(t)|^2\, dt = +\infty \quad \text{or} \quad \int_{-\infty}^{+\infty} \omega^2 |\hat{g}(\omega)|^2\, d\omega = +\infty. \qquad (5.91)$$

This theorem proves that we cannot construct an orthogonal windowed Fourier basis with a differentiable window g of compact support. On the other hand, one can verify that the discontinuous rectangular window

$$g = \frac{1}{\sqrt{u_0}}\, \mathbf{1}_{[-u_0/2,u_0/2]}$$

yields an orthogonal windowed Fourier basis for $u_0\xi_0 = 2\pi$. This basis is rarely used because of the bad frequency localization of $\hat{g}$.

Sufficient Conditions

Theorem 5.21 proved by Daubechies [195] gives sufficient conditions on u_0, ξ_0, and g for constructing a windowed Fourier frame.

Theorem 5.21: *Daubechies.* Let us define

$$\theta(u) = \sup_{0\leqslant t\leqslant u_0} \sum_{n=-\infty}^{+\infty} |g(t - nu_0)|\, |g(t - nu_0 + u)| \qquad (5.92)$$

and

$$\Delta = \sum_{\substack{k=-\infty \\ k\neq 0}}^{+\infty} \left[\theta\left(\frac{2\pi k}{\xi_0}\right) \theta\left(\frac{-2\pi k}{\xi_0}\right) \right]^{1/2}. \qquad (5.93)$$

If u_0 and ξ_0 satisfy

$$A_0 = \frac{2\pi}{\xi_0} \left(\int_{0\leqslant t\leqslant u_0} \sum_{n=-\infty}^{+\infty} |g(t - nu_0)|^2 - \Delta \right) > 0 \qquad (5.94)$$

and

$$B_0 = \frac{2\pi}{\xi_0} \left(\sup_{0\leqslant t\leqslant u_0} \sum_{n=-\infty}^{+\infty} |g(t - nu_0)|^2 + \Delta \right) < +\infty, \qquad (5.95)$$

then $\{g_{n,k}\}_{(n,k)\in\mathbb{Z}^2}$ is a frame. The constants A_0 and B_0 are, respectively, lower bounds and upper bounds of the frame bounds A and B.

Observe that the only difference between the sufficient conditions (5.94, 5.95) and the necessary condition (5.89) is the addition and subtraction of Δ. If Δ is small compared to $\inf_{0\leqslant t\leqslant u_0} \sum_{n=-\infty}^{+\infty} |g(t - nu_0)|^2$, then A_0 and B_0 are close to the optimal frame bounds A and B.

Dual Frame

Theorem 5.5 proves that the dual-windowed frame vectors are

$$\tilde{g}_{n,k} = (\Phi^*\Phi)^{-1}g_{n,k}. \tag{5.96}$$

Theorem 5.22 shows that this dual frame is also a windowed Fourier frame, which means that its vectors are time and frequency translations of a new window $\tilde{g}$.

Theorem 5.22. Dual-windowed Fourier vectors can be rewritten as

$$\tilde{g}_{n,k}(t) = \tilde{g}(t - nu_0)\,\exp(ik\xi_0 t),$$

where $\tilde{g}$ is the dual window

$$\tilde{g} = (\Phi^*\Phi)^{-1}g. \tag{5.97}$$

Proof. This result is proved by showing first that $\Phi^*\Phi$ commutes with time and frequency translations proportional to u_0 and ξ_0. If $\phi \in \mathbf{L}^2(\mathbb{R})$ and $\phi_{m,l}(t) = \phi(t - mu_0)\,\exp(il\xi_0 t)$, we verify that

$$\Phi^*\Phi\phi_{m,l}(t) = \exp(il\xi_0 t)\,\Phi^*\Phi h(t - mu_0).$$

Indeed,

$$\Phi^*\Phi\phi_{m,l} = \sum_{(n,k)\in\mathbb{Z}^2} \langle \phi_{m,l}, g_{n,k}\rangle\, g_{n,k}$$

and a change of variable yields

$$\langle \phi_{m,l}, g_{n,k}\rangle = \langle \phi, g_{n-m,k-l}\rangle.$$

Consequently,

$$\Phi^*\Phi\phi_{m,l}(t) = \sum_{(n,k)\in\mathbb{Z}^2} \langle \phi, g_{n-m,k-l}\rangle\,\exp(il\xi_0 t)\,g_{n-m,k-l}(t - mu_0)$$

$$= \exp(il\xi_0 t)\,\Phi^*\Phi\phi(t - mu_0).$$

Since $\Phi^*\Phi$ commutes with these translations and frequency modulations, we verify that $(\Phi^*\Phi)^{-1}$ necessarily commutes with the same group operations. Thus,

$$\tilde{g}_{n,k}(t) = (\Phi^*\Phi)^{-1}g_{n,k} = \exp(ik\xi_0)\,(\Phi^*\Phi)^{-1}g_{0,0}(t - nu_0) = \exp(ik\xi_0)\,\tilde{g}(t - nu_0). \qquad \blacksquare$$

Gaussian Window

The Gaussian window

$$g(t) = \pi^{-1/4}\,\exp\left(\frac{-t^2}{2}\right) \tag{5.98}$$

has a Fourier transform $\hat{g}$ that is a Gaussian with the same variance. The time and frequency spreads of this window are identical. Therefore, let us choose equal sampling intervals in time and frequency: $u_0 = \xi_0$. For the same product $u_0\xi_0$ other

Table 5.3 Frame Bounds for the Gaussian Window (5.98) and $u_0 = \xi_0$

$u_0\xi_0$	A_0	B_0	B_0/A_0
$\pi/2$	3.9	4.1	1.05
$3\pi/4$	2.5	2.8	1.1
π	1.6	2.4	1.5
$4\pi/3$	0.58	2.1	3.6
1.9π	0.09	2.0	22

choices would degrade the frame bounds. If g is dilated by s then the time and frequency sampling intervals must become su_0 and ξ_0/s.

If the time-frequency sampling density is above the critical value of $2\pi/(u_0\xi_0) > 1$, then Daubechies [195] proves that $\{g_{n,k}\}_{(n,k)\in\mathbb{Z}^2}$ is a frame. When $u_0\xi_0$ tends to 2π, the frame bound A tends to 0. For $u_0\xi_0 = 2\pi$, the family $\{g_{n,k}\}_{(n,k)\in\mathbb{Z}^2}$ is complete in $\mathbf{L}^2(\mathbb{R})$, which means that any $f \in \mathbf{L}^2(\mathbb{R})$ is entirely characterized by the inner products $\{\langle f, g_{n,k}\rangle\}_{(n,k)\in\mathbb{Z}^2}$. However, the Balian-Low theorem (5.20) proves that it cannot be a frame and one can indeed verify that $A = 0$ [195]. This means that the reconstruction of f from these inner products is unstable.

Table 5.3 gives the estimated frame bounds A_0 and B_0 calculated with Theorem 5.21, for different values of $u_0 = \xi_0$. For $u_0\xi_0 = \pi/2$, which corresponds to time and frequency sampling intervals that are half the critical sampling rate, the frame is nearly tight. As expected, $A \approx B \approx 4$, which verifies that the redundancy factor is 4 (2 in time and 2 in frequency). Since the frame is almost tight, the dual frame is approximately equal to the original frame, which means that $\tilde{g} \approx g$. When $u_0\xi_0$ increases we see that A decreases to zero and $\tilde{g}$ deviates more and more from a Gaussian. In the limit $u_0\xi_0 = 2\pi$, the dual window $\tilde{g}$ is a discontinuous function that does not belong to $\mathbf{L}^2(\mathbb{R})$. These results can be extended to discrete windowed Fourier transforms computed with a discretized Gaussian window [501].

5.5 MULTISCALE DIRECTIONAL FRAMES FOR IMAGES

To reveal geometric image properties, wavelet frames are constructed with mother wavelets having a direction selectivity, providing information on the direction of sharp transitions such as edges and textures. Directional wavelet frames are described in Section 5.5.1.

Wavelet frames yield high-amplitude coefficients in the neighborhood of edges, and cannot take advantage of their geometric regularity to improve the sparsity of the representation. Curvelet frames, described in Section 5.5.2, are constructed with elongated waveforms that follow directional image structures and improve the representation sparsity.

5.5.1 Directional Wavelet Frames

A directional wavelet transform decomposes images over directional wavelets that are translated, rotated, and dilated at dyadic scales. Such transforms appear in many image-processing applications and physiological models. Applications to texture discrimination are also discussed.

A directional wavelet $\psi^\alpha(x)$ with $x = (x_1, x_2) \in \mathbb{R}^2$ of angle α is a wavelet having p directional vanishing moments along any one-dimensional line of direction $\alpha + \pi/2$ in the plane

$$\forall \rho \in \mathbb{R}, \quad \int \psi^\alpha(\rho \cos \alpha - u \sin \alpha, \rho \sin \alpha + u \cos \alpha) \, u^k \, du = 0 \quad \text{for} \quad 0 \leqslant k < p, \quad \textbf{(5.99)}$$

but does not have directional vanishing moments along the direction α. Such a wavelet oscillates in the direction of $\alpha + \pi/2$ but not in the direction α. It is orthogonal to any two-dimensional polynomial of degree strictly smaller than p (Exercise 5.21).

The set Θ of chosen directions are typically uniform in $[0, \pi]$: $\Theta = \{\alpha = k\pi/K \text{ for } 0 \leqslant k < K\}$. Dilating these directional wavelets by factors 2^j and translating them by any $u \in \mathbb{R}$ yields a translation-invariant directional wavelet family:

$$\{\psi_{2^j}^\alpha(x - u)\}_{u \in \mathbb{R}^2, j \in \mathbb{Z}, \alpha \in \Theta} \quad \text{with} \quad \psi_{2^j}^\alpha(x) = 2^{-j} \psi^\alpha(2^{-j}x). \quad \textbf{(5.100)}$$

Directional wavelets may be derived by rotating a single mother wavelet $\psi(x_1, x_2)$ having vanishing moments in the horizontal direction, with a rotation operator R_α of angle α in $\mathbb{R}^2$.

A dyadic directional wavelet transform of f computes the inner product with each wavelet:

$$W f(u, 2^j, \alpha) = \langle f, \psi_{2^j, u}^\alpha \rangle \quad \text{where} \quad \psi_{2^j, u}^\alpha(x) = \psi_{2^j}^\alpha(x - u).$$

This dyadic wavelet transform can also be written as convolutions with directional wavelets:

$$W f(u, 2^j, \alpha) = f \star \bar{\psi}_{2^j}^\alpha(u) \quad \text{where} \quad \bar{\psi}_{2^j}^\alpha(x) = \psi_{2^j}^\alpha(-x).$$

A wavelet $\psi_{2^j}^\alpha(x - u)$ has a support dilated by 2^j, located in the neighborhood of u and oscillates in the direction of $\alpha + \pi/2$. If $f(x)$ is constant over the support of $\psi_{2^j, u}^\alpha$ along lines of direction $\alpha + \pi/2$, then $\langle f, \psi_{2^j, u}^\alpha \rangle = 0$ because of its directional vanishing moments. In particular, this coefficient vanishes in the neighborhood of an edge having a tangent in the direction $\alpha + \pi/2$. If the edge angle deviates from $\alpha + \pi/2$, then it produces large amplitude coefficients, with a maximum typically when the edge has a direction α. Thus, the amplitude of wavelet coefficients depends on the local orientation of the image structures.

Theorem 5.11 proves that the translation-invariant wavelet family is a frame if there exists $B \geqslant A > 0$ such that the generators $\phi_n(x) = 2^{-j}\psi_{2^j}^{\alpha}(x)$ have Fourier transforms $\hat{\phi}_n(\omega) = \hat{\psi}^{\alpha}(\omega)$, which satisfy

$$\forall \omega = (\omega_1, \omega_2) \in \mathbb{R}^2 - \{(0,0)\}, \quad A \leqslant \sum_{\alpha \in \Theta} \sum_{j=-\infty}^{+\infty} |\hat{\psi}^{\alpha}(2^j\omega)|^2 \leqslant B. \tag{5.101}$$

It results from Theorem 5.11 that there exists a dual family of reconstructing wavelets $\{\tilde{\psi}^{\alpha}\}_{\alpha \in \Theta}$ that have Fourier transforms that satisfy

$$\sum_{j=-\infty}^{+\infty} \sum_{\alpha \in \Theta} \widehat{\tilde{\psi}^{\alpha}}(2^j\omega)\, \widehat{\psi}^{\alpha*}(2^j\omega) = 1, \tag{5.102}$$

which yields

$$f(x) = \sum_{j=-\infty}^{+\infty} \frac{1}{2^{2j}} \sum_{\alpha \in \Theta} Wf(\cdot, 2^j, \alpha) \star \tilde{\psi}_{2^j}^{\alpha}(x). \tag{5.103}$$

Examples of directional wavelets obtained by rotating a single mother wavelet are constructed with Gabor functions and steerable derivatives.

Gabor Wavelets

In the cat's visual cortex, Hubel and Wiesel [306] discovered a class of cells, called simple cells, having a response that depends on the frequency and direction of the visual stimuli. Numerous physiological experiments [401] have shown that these cells can be modeled as linear filters with impulse responses that have been measured at different locations of the visual cortex. Daugmann [200] showed that these impulse responses can be approximated by *Gabor wavelets*, obtained with a Gaussian window $g(x_1, x_2) = (2\pi)^{-1}e^{-(x_1^2+x_2^2)/2}$ multiplied by a sinusoidal wave:

$$\psi^{\alpha}(x_1, x_2) = g(x_1, x_2)\, \exp[-i\eta(-x_1 \sin\alpha + x_2 \cos\alpha)]. \tag{5.104}$$

These findings suggest the existence of some sort of wavelet transform in the visual cortex, combined with subsequent nonlinearities [403]. The "physiological" wavelets have a frequency resolution on the order of 1 to 1.5 octaves, and are thus similar to dyadic wavelets.

The Fourier transform of $g(x_1, x_2)$ is $\hat{g}(\omega_1, \omega_2) = e^{-(\omega_1^2+\omega_2^2)/2}$. It results from (5.104) that

$$\hat{\psi}_{2^j}^{\alpha}(\omega_1, \omega_2) = \sqrt{2^j}\, \hat{g}(2^j\omega_1 + \eta\sin\alpha, 2^j\omega_2 - \eta\cos\alpha).$$

In the Fourier plane, the energy of this Gabor wavelet is mostly concentrated around $(-2^{-j}\eta\sin\alpha, 2^{-j}\eta\cos\alpha)$, in a neighborhood proportional to 2^{-j}.
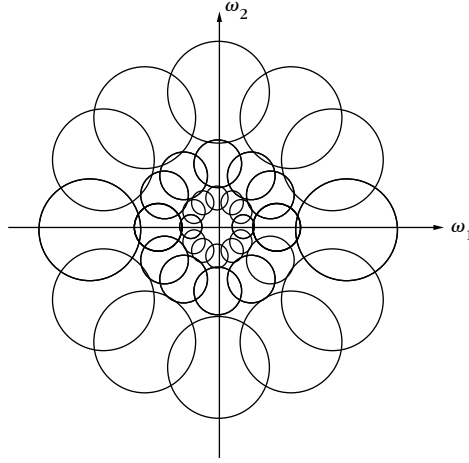
FIGURE 5.8

Each circle represents the frequency domain in a direction $\alpha + \pi/2$ where the amplitude of a Gabor wavelet Fourier transform $|\hat{\psi}_{2^j}^{\alpha}(\omega)|$ is large. It is proportional to 2^{-j} and its position rotates with α.

The direction is chosen to be uniform $\alpha = l\pi/K$ for $-K < l \leqslant K$. Figure 5.8 shows a cover of the frequency plane by dyadic Gabor wavelets 5.105 with $K = 6$. If $K \geqslant 4$ and η is of the order of 1 then 5.101 is satisfied with stable bounds. Since images $f(x)$ are real, $\hat{f}(-\omega) = \hat{f}^*(\omega)$ and f can be reconstructed by covering only half of the frequency plane, with $-K < l \leqslant 0$. This is a two-dimensional equivalent of the one-dimensional analytic wavelet transform, studied in Section 4.3.2, with wavelets having a Fourier transform support restricted to positive frequencies. For texture analysis, Gabor wavelets provide information on the local image frequencies.

Texture Discrimination

Despite many attempts, there are no appropriate mathematical models for "homogeneous image textures." The notion of texture homogeneity is still defined with respect to our visual perception. A texture is said to be homogeneous if it is preattentively perceived as being homogeneous by a human observer.

The texton theory of Julesz [322] was a first important step in understanding the different parameters that influence the perception of textures. The direction of texture elements and their frequency content seem to be important clues for discrimination. This motivated early researchers to study the repartition of texture energy in the Fourier domain [92]. For segmentation purposes it is necessary to localize texture measurements over neighborhoods of varying sizes. Thus, the Fourier transform was replaced by localized energy measurements at the output of filter banks that compute a wavelet transform [315, 338, 402, 467]. Besides the algorithmic efficiency of this approach, this model is partly supported by physiological studies of the visual cortex.

Since $Wf(u, 2^j, \alpha) = f \star \bar{\psi}_{2^j}^\alpha(u)$, Gabor wavelet coefficients measure the energy of f in a spatial neighborhood of u of size 2^j, and in a frequency neighborhood of $(-2^{-j}\eta \sin \alpha, 2^{-j}\eta \cos \alpha)$ of size 2^{-j}, where the support of $\hat{\psi}_{2^j}^\alpha(\omega)$ is located, illustrated in Figure 5.8. Varying the scale 2^j and the angle α modifies the frequency channel [119]. The wavelet transform energy $|Wf(u, 2^j, \alpha)|^2$ is large when the angle α and scale 2^j match the direction and scale of high-energy texture components in the neighborhood of u. Thus, the amplitude of $|Wf(u, 2^j, \alpha)|^2$ can be used to discriminate textures. Figure 5.9 shows the dyadic wavelet transform of two textures, computed along horizontal and vertical directions, at the scales 2^{-4} and 2^{-5} (the image support is normalized to $[0, 1]^2$). The central texture is regular vertically and has more energy along horizontal high frequencies than the peripheric texture. These two textures are therefore discriminated by the wavelet of angle $\alpha = \pi/2$, whereas the other wavelet with $\alpha = 0$ produces similar responses for both textures.

For segmentation, one must design an algorithm that aggregates the wavelet responses at all scales and directions in order to find the boundaries of homogeneous textured regions. Both clustering procedures and detection of sharp transitions over wavelet energy measurements have been used to segment the image [315, 402, 467]. These algorithms work well experimentally but rely on ad hoc parameter settings.
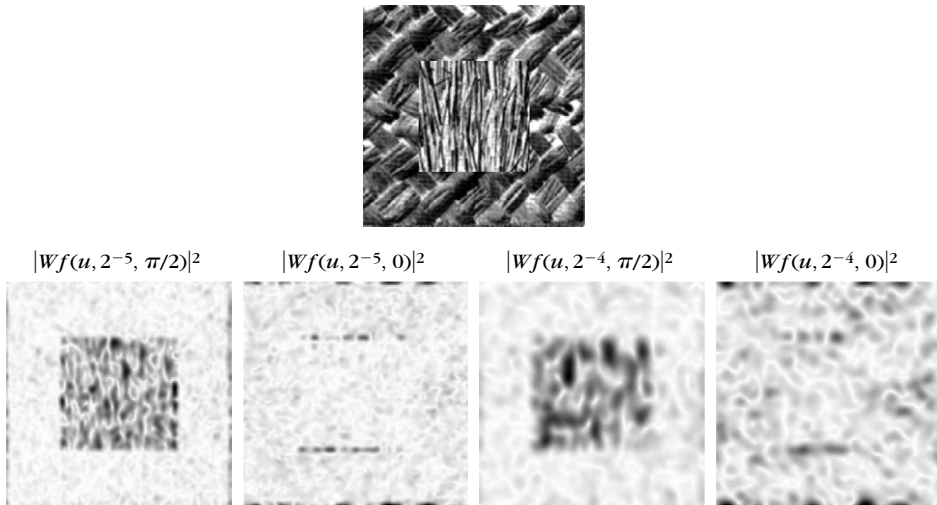

$|Wf(u, 2^{-5}, \pi/2)|^2$ $|Wf(u, 2^{-5}, 0)|^2$ $|Wf(u, 2^{-4}, \pi/2)|^2$ $|Wf(u, 2^{-4}, 0)|^2$

FIGURE 5.9

Directional Gabor wavelet transform $|Wf(u, 2^j, \alpha)|^2$ of a texture patch, at the scales $2^j = 2^{-4}, 2^{-5}$, along two directions $\alpha = 0, \pi/2$. The darker the pixel, the larger the wavelet coefficient amplitude.

Steerable Wavelets

Steerable directional wavelets along any angle α can be written as a linear expansion of few mother wavelets [441]. For example, a steerable wavelet in the direction α can be defined as the partial derivative of order p of a window $\flat(x)$ in the direction of the vector $\vec{n} = (-\sin\alpha, \cos\alpha)$:

$$\psi^\alpha(x) = \frac{\partial^p \theta(x)}{\partial \vec{n}^p} = \left(-\sin\alpha \frac{\partial}{\partial x_1} + \cos\alpha \frac{\partial}{\partial x_2}\right)^p \theta(x). \tag{5.105}$$

Let R_α be the planar rotation by an angle α. If the window is invariant under rotations $\theta(x) = \theta(R_\alpha x)$, then these wavelets are generated by the rotation of a single mother wavelet: $\psi^\alpha(x) = \psi(R_\alpha x)$ with $\psi = \partial^p \theta / \partial x_2^p$.

Furthermore, the expansion of the derivatives in (5.105) proves that each ψ^α can be expressed as a linear combination of $p + 1$ partial derivatives

$$\psi^\alpha(x) = \sum_{i=0}^{p} a_i(\alpha)\,\rho^i(x), \quad \text{where} \quad a_i(\alpha) = \binom{p}{i}(-\sin\alpha)^i (\cos\alpha)^{p-i}, \tag{5.106}$$

with

$$\forall\, 0 \leqslant i \leqslant p, \quad \rho^i(x) = \frac{\partial^p \theta(x)}{\partial x_1^i\, \partial x_2^{p-i}}.$$

The waveforms $\rho^i(x)$ can also be considered as wavelets functions with vanishing moments. It results from 5.106 that the directional wavelet transform at any angle α can be calculated from $p + 1$ convolutions of f with the ρ^i dilated:

$$Wf(u, 2^j, \alpha) = \sum_{i=0}^{p} a_i(\alpha)(f \star \bar{\rho}_{2^j}^i)(u) \quad \text{for} \quad \bar{\rho}_{2^j}^i(x) = 2^{-j}\rho^i(-2^{-j}x).$$

Exercise 5.22 gives conditions on θ so that for a set Θ of $p + 1$ angles $\alpha = k\pi/(p+1)$ with $0 \leqslant k < p$ the resulting oriented wavelets ψ^α define a family of dyadic wavelets that satisfy 5.101. Section 6.3 uses such directional wavelets, with $p = 1$, to detect multiscale edges in images.

Discretization of the Translation

A translation-invariant wavelet transforms $Wf(u, 2^j, \alpha)$ for all scales 2^j, and angle α requires a large amount of memory. To reduce computation and memory storage, the translation parameter is discretized. In the one-dimensional case a frame is obtained by uniformly sampling the translation parameter u with intervals $u_0 2^j n$ with $n = (n_1, n_2) \in \mathbb{Z}^2$, proportional to the scale 2^j. The discretized wavelet derived from the translation-invariant wavelet family (5.100) is

$$\{\psi_{2^j}^\alpha(x - 2^j u_0 n)\}_{n \in \mathbb{Z}^2, j \in \mathbb{Z}, \alpha \in \Theta} \quad \text{with} \quad \psi_{2^j}^\alpha(x) = 2^{-j}\psi^\alpha(2^{-j}x). \tag{5.107}$$

Necessary and sufficient conditions similar to Theorems 5.15 and 5.16 can be established to guarantee that such a wavelet family defines a frame of $\mathbf{L}^2(\mathbb{R}^2)$.

To decompose images in such wavelet frames with a fast filter filter bank, directional wavelets can be synthesized as a product of discrete filters. The steerable pyramid of Simoncelli et al. [441] decomposes images in such a directional wavelet frame, with a cascade of convolutions with low-pass filters and directional band-pass filters. The filter coefficients are optimized to yield wavelets that satisfy approximately the steerability condition 5.106 and produce a tight frame. The sampling interval is $u_0 = 1/2$.

Figure 5.10 shows an example of decomposition on such a steerable pyramid with $K = 4$ directions. For discrete images of N pixels, the finest scale is $2^j = 2N^{-1}$. Since $u_0 = 1/2$, wavelet coefficients at the finest scale define an image of N pixels for each direction. The wavelet image size then decreases as the scale 2^j increases. The total number of wavelet coefficients is $4KN/3$ and the tight frame factor is $4K/3$ [441]. Steerable wavelet frames are used to remove noise with wavelet thresholding estimators [404] and for texture analysis and synthesis [438].

Chapter 9 explains that sparse image representation can be obtained by keeping large-amplitude coefficients above a threshold. Large-amplitude wavelet coefficients appear where the image has a sharp transition, when the wavelet oscillates in a direction approximately perpendicular to the direction of the edge. However, even when directions are not perfectly aligned, wavelet coefficients remain nonnegligible in the neighborhood of edges. Thus, the number of large-amplitude wavelet coefficients is typically proportional to the length of edges in images. Reducing the number of large coefficients requires using waveforms that are more sensitive to direction properties, as shown in the next section.

5.5.2 Curvelet Frames

Curvelet frames were introduced by Candès and Donoho [134] to construct sparse representation for images including edges that are geometrically regular. Similar to directional wavelets, curvelet frames are obtained by rotating, dilating, and translating elementary waveforms. However, curvelets have a highly elongated support obtained with a parabolic scaling using different scaling factors along the curvelet width and length. These anisotropic waveforms have a much better direction sensitivity than directional wavelets. Section 9.3.2 studies applications to sparse approximations of geometrically regular images.

Dyadic Curvelet Transform
A curvelet is function $c(x)$ having vanishing moments along the horizontal direction like a wavelet. However, as opposed to wavelets, dilated curvelets are obtained with a parabolic scaling law that produces highly elongated waveforms at fine scales:

$$c_{2^j}(x_1, x_2) \approx 2^{-3j/4} c(2^{-j/2}x_1, 2^{-j}x_2). \tag{5.108}$$

They have a *width* proportional to their *length*^{2}. Dilated curvelets are then rotated $c_{2^j}^\alpha = c_{2^j}(R_\alpha x)$, where R_α is the planar rotation of angle α, and translated like wavelets:

Image f

$\alpha = \pi/2$ $\alpha = 3\pi/4$ $\alpha = 0$ $\alpha = \pi/4$

FIGURE 5.10

Decomposition of an image in a frame of steerable directional wavelets [441] along four directions: $\alpha = 0, \pi/4, \pi/2, 3\pi/4$, at two consecutive scales, 2^j and $2^j + 1$. Black, gray, and white pixels correspond respectively to wavelet coefficients of negative, zero, and positive values.

$c_{2^j,u}^\alpha = c_{2^j}^\alpha(x - u)$. The resulting translation-invariant dyadic curvelet transform of $f \in \mathbf{L}^2(\mathbb{R}^2)$ is defined by

$$Cf(u, 2^j, \alpha) = \langle f, c_{2^j,u}^\alpha \rangle = f \star \bar{c}_{2^j}^\alpha(u) \quad \text{with} \quad \bar{c}_{2^j}^\alpha(x) = c_{2^j}^\alpha(-x).$$

To obtain a tight frame, the Fourier transform of a curvelet at a scale 2^j is defined by

$$\hat{c}_{2^j}(\omega) = 2^{3j/4} \hat{\psi}(2^j r) \hat{\phi}\left(\frac{2\theta}{2^{\lfloor j/2 \rfloor}\pi}\right), \quad \text{with} \quad \omega = r(\cos\theta, \sin\theta), \tag{5.109}$$
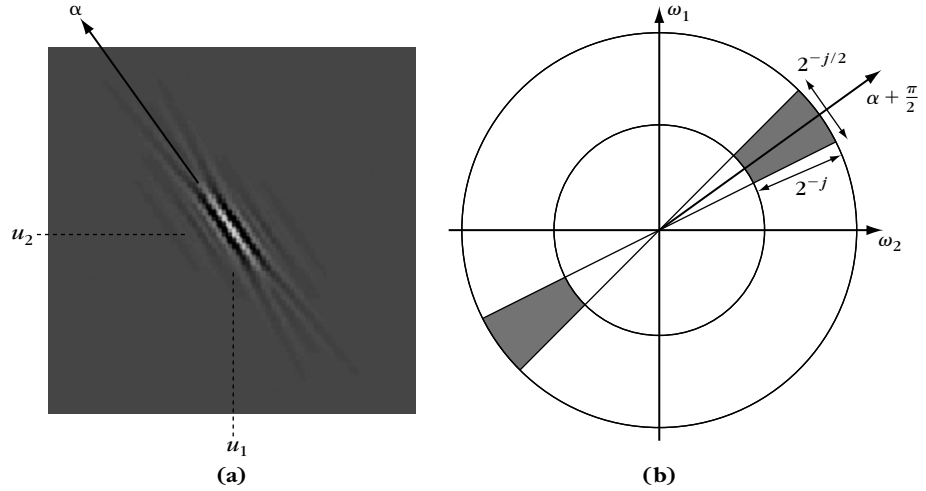
FIGURE 5.11

(a) Example of curvelet $c_{2^j,u}^{\alpha}(x)$. **(b)** The frequency support of $\hat{c}_{2^j,u}^{\alpha}(\omega)$ is a wedge obtained as a product of a radial window with an angular window.

where $\hat{\psi}$ is the Fourier transform of a one-dimensional wavelet and $\hat{\phi}$ is a one-dimensional angular window that localizes the frequency support of $\hat{c}_{2^j}$ in a polar parabolic wedge, illustrated in Figure 5.11. The wavelet $\hat{\psi}$ is chosen to have a compact support in $[1/2, 2]$ and satisfies the dyadic frequency covering:

$$\forall\, r \in \mathbb{R}^*, \quad \sum_{j=-\infty}^{+\infty} |\hat{\psi}(2^j r)|^2 = 1. \tag{5.110}$$

One may, for example, choose a Meyer wavelet as defined in (7.82). The angular window $\hat{\phi}$ is chosen to be supported in $[-1, 1]$ and satisfies

$$\forall\, u, \quad \sum_{k=-\infty}^{+\infty} |\hat{\phi}(u-k)|^2 = 1. \tag{5.111}$$

As a result of these two properties, one can verify that for uniformly distributed angles,

$$\Theta_j = \{\alpha = k\pi 2^{\lfloor j/2 \rfloor - 1} \quad \text{for} \quad 0 \leqslant k < 2^{-\lfloor j/2 \rfloor + 2}\}$$

curvelets cover the frequency plane

$$\forall\, \omega \in \mathbb{R}^2 - \{0\}, \quad \sum_{j \in \mathbb{Z}} \sum_{\alpha \in \Theta_j} 2^{-3j/2} |\hat{c}_{2^j}^{\alpha}(\omega)|^2 = 1. \tag{5.112}$$

Real valued curvelets are obtained with a symmetric version of 5.109: $\hat{c}_{2^j}(\omega) + \hat{c}_{2^j}(-\omega)$. Applying Theorem 5.11 proves that a translation-invariant dyadic curvelet dictionary $\{c_{2^j,u}^\alpha\}_{\alpha\in\Theta_j, j\in\mathbb{Z}, u\in\mathbb{R}^2}$ is a dyadic translation-invariant tight frame that defines a complete and stable signal representation [142].

Theorem 5.23: *Candès, Donoho.* For any $f \in \mathbf{L}^2(\mathbb{R}^2)$,

$$\|f\|^2 = \sum_{j\in\mathbb{Z}} 2^{-3j/2} \sum_{\alpha\in\Theta_j} \|Cf(\cdot, 2^j, \alpha)\|^2,$$

and

$$f(x) = \sum_{j\in\mathbb{Z}} 2^{-3j/2} \sum_{\alpha\in\Theta_j} Cf(\cdot, 2^j, \alpha) * c_{2^j}^\alpha(x).$$

Curvelet Properties

Since $\hat{c}_{2^j}(\omega)$ is a smooth function with a support included in a rectangle of size proportional to $2^{-j/2} \times 2^{-j}$, the spatial curvelet $c_{2^j}(x)$ is a regular function with a fast decay outside a rectangle of size $2^{j/2} \times 2^j$. The rotated and translated curvelet $c_{2^j,u}^\alpha$ is supported around the point u in an elongated rectangle along the direction α; its shape has a parabolic ratio $width = length^2$, as shown in Figure 5.11.

Since the Fourier transform $\hat{c}_{2^j}(\omega_1, \omega_2)$ is zero in the neighborhood of the vertical axis $\omega_1 = 0$, $c_{2^j}(x_1, x_2)$ has an infinite number of vanishing moments in the horizontal direction

$$\forall \omega_1, \quad \frac{\partial^q \hat{c}_j}{\partial^q \omega_1}(0, \omega_1) = 0 \quad \Rightarrow \quad \forall q \geqslant 0, \quad \forall x_2, \quad \int c_{2^j}(x_1, x_2) x_1^q dx_1 = 0.$$

A rotated curvelet $c_{2^j,u}^\alpha$ has vanishing moments in the direction $\alpha + \pi/2$, and therefore oscillates in the direction $\alpha + \pi/2$, whereas its support is elongated in the direction α.

Discretization of Translation

Curvelet tight frames are constructed by sampling the translation parameter u [134]. These tight frames provide sparse representations of signals including regular geometric structures.

The curvelet sampling grid depends on the scale 2^j and on the angle α. Sampling intervals are proportional to the curvelet width 2^j in the direction $\alpha + \pi/2$ and to its length $2^{j/2}$ in the direction α:

$$\forall m = (m_1, m_2) \in \mathbb{Z}^2, \quad u_m^{(j,\alpha)} = R_\alpha(2^{j/2}m_1, 2^j m_2). \tag{5.113}$$

Figure 5.12 illustrates this sampling grid. The resulting dictionary of translated curvelets is

$$\left\{ c_{j,m}^\alpha(x) = c_{2^j}^\alpha(x - u_m^{(j,\alpha)}) \right\}_{j\in\mathbb{Z}, \alpha\in\Theta_j, m\in\mathbb{Z}^2}.$$

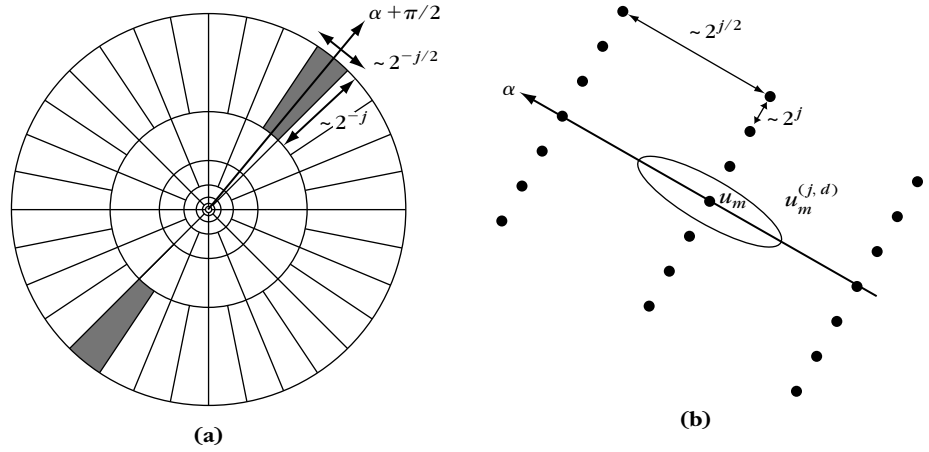**FIGURE 5.12**

(a) Curvelet polar tiling of the frequency plane with parabolic wedges. **(b)** Curvelet spatial sampling grid $u_m^{(j,\alpha)}$ at a scale 2^j and direction α.

Theorem 5.24 proves that this curvelet family is a tight frame of $\mathbf{L}^2(\mathbb{R}^2)$. The proof is not given here, but can be found in [142].

Theorem 5.24: *Candès, Donoho.* For any $f \in \mathbf{L}^2(\mathbb{R}^2)$,

$$\|f\|^2 = \sum_{j \in \mathbb{Z}} \sum_{\alpha \in \Theta_j} \sum_{m \in \mathbb{Z}^2} |\langle f, c_{j,m}^\alpha \rangle|^2 \qquad (5.114)$$

and

$$f(x) = \sum_{j \in \mathbb{Z}} \sum_{\alpha \in \Theta_j} \sum_{m \in \mathbb{Z}^2} \langle f, c_{j,m}^\alpha \rangle c_{j,m}^\alpha(x).$$

Wavelet versus Curvelet Coefficients

In the neighborhood of an edge having a tangent in a direction θ, large-amplitude coefficients are created by curvelets and wavelets of direction $\alpha = \theta$, which have their vanishing moment in the direction $\theta + \pi/2$. These curvelets have a support elongated in the edge direction θ, as illustrated in Figure 5.13. In this direction, the sampling grid of a curvelet frame has an interval $2^{j/2}$, which is much larger than the sampling interval 2^j of a wavelet frame. Thus, an edge is covered by fewer curvelets than wavelets having a direction equal to the edge direction. If the angle α of the curvelet deviates from θ, then curvelet coefficients decay quickly because of the narrow frequency localizaton of curvelets. This gives a high-directional selectivity to curvelets.
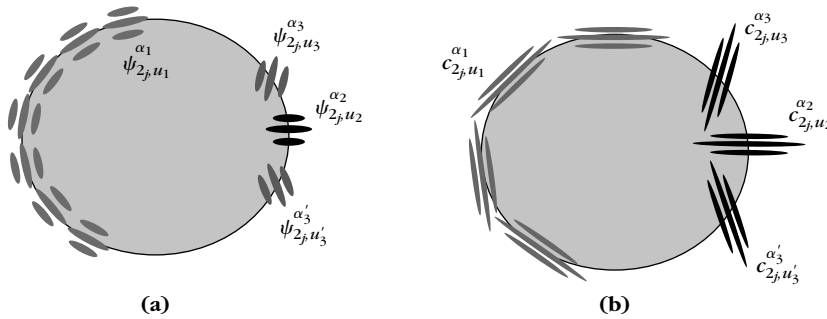
FIGURE 5.13

(a) Directional wavelets: a regular edge creates more large-amplitude wavelet coefficients than curvelet coefficients. **(b)** Curvelet coefficients have a large amplitude when their support is aligned with the edge direction, but there are few such curvelets.

Even though wavelet coefficients vanish when $\alpha = \theta + \pi/2$, they have a smaller directional selectivity than curvelets, and wavelet coefficients' amplitudes decay more slowly as α deviates from θ. Indeed, the frequency support of wavelets is much wider and their spatial support is nearly isotropic. As a consequence, an edge produces large-amplitude wavelet coefficients in several directions. This is illustrated by Figure 5.10, where Lena's shoulder edge creates large coefficients in three directions, and small coefficients only when the wavelet and the edge directions are aligned.

As a result, edges and image structures with some directional regularity create fewer large-amplitude curvelet coefficients than wavelet coefficients. The theorem derived from Section 9.3.3 proves that for images having regular edges, curvelet tight frames are asymptotically more efficient than wavelet bases when building sparse representations.

Fast Curvelet Decomposition Algorithm

To compute the curvelet transform of a discrete image $f[n_1, n_2]$ uniformly sampled over N pixels, one must take into account the discretization grid, which imposes constraints on curvelet angles. The fast curvelet transform [140] replaces the polar tiling of the Fourier domain by a recto-polar tiling, illustrated in Figure 5.14(b). The directions α are uniformly discretized so that the slopes of the wedges containing the support of the curvelets are uniformly distributed in each of the north, south, west, and east Fourier quadrants. Each wedge is the support of the two-dimensional DFT $\hat{c}_j^\alpha[k_1, k_2]$ of a discrete curvelet $c_j^\alpha[n_1, n_2]$. The curvelet translation parameters are not chosen according to 5.113, but remain on a subgrid of the original image sampling grid. At a scale 2^j, there is one sampling grid $(2^{\lfloor j/2 \rfloor} m_1, 2^j m_2)$ for curvelets in the east and west quadrants. In these directions, curvelet coefficients are

$$\langle f[n_1, n_2], c_j^\alpha[n_1 - 2^{\lfloor j/2 \rfloor} m_1, n_2 - 2^j m_2] \rangle = f \star \bar{c}_j^\alpha[2^{\lfloor j/2 \rfloor} m_1, 2^j m_2] \qquad \textbf{(5.115)}$$
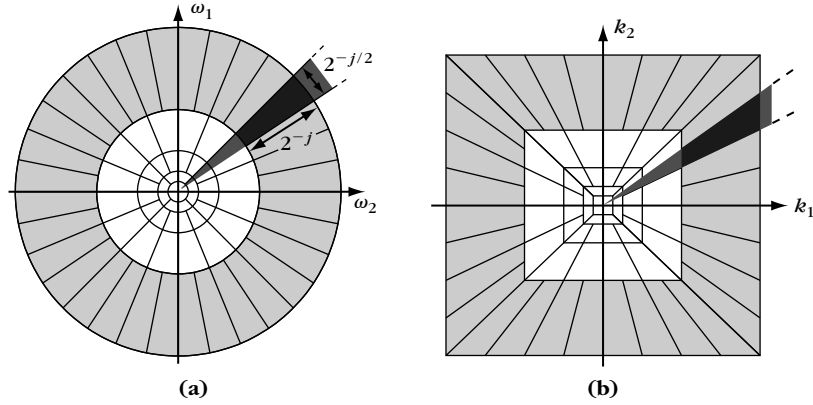
FIGURE 5.14

(a) Curvelet frequency plane tiling. The dark gray area is a wedge obtained as the product of a radial window and an angular window. **(b)** Discrete curvelet frequency tiling. The radial and angular windows define trapezoidal wedges as shown in dark gray.

with $\bar{c}_j^\alpha[n_1, n_2] = c_j^\alpha[-n_1, -n_2]$. For curvelets in the north and south quadrants the translation grid is $(2^j m_1, 2^{\lfloor j/2 \rfloor} m_2)$, which corresponds to curvelet coefficients

$$\langle f[n_1, n_2], c_j^\alpha[n_1 - 2^j m_1, n_2 - 2^{\lfloor j/2 \rfloor} m_2] \rangle = f \star \bar{c}_j^\alpha[2^j m_1, 2^{\lfloor j/2 \rfloor} m_2]. \qquad \textbf{(5.116)}$$

The discrete curvelet transform computes the curvelet filtering and sampling with a two-dimensional FFT. The two-dimensional discrete Fourier transforms of $f[n]$ and $\bar{c}_j^\alpha[n]$ are $\hat{c}_j^\alpha[-k]$ and $\hat{f}[k]$. The algorithm proceeds as:

- Computation of the two-dimensional DFT $\hat{f}[k]$ of $f[n]$.
- For each j and the corresponding $2^{-\lfloor j/2 \rfloor + 2}$ angles α, calculation of $\hat{f}[k]\,\hat{c}_j^\alpha[-k]$.
- Computation of the inverse Fourier transform of $\hat{f}[k]\,\hat{c}_j^\alpha[-k]$ on the smallest possible warped frequency rectangle including the wedge support of $\hat{c}_j^\alpha[-k]$.

The critical step is the last inverse Fourier transform. A computationally more expensive one would compute $f \star \bar{c}_j^\alpha[n]$ for all $n = (n_1, n_2)$ and then subsample this convolution along the grids (5.115) and (5.116).

Instead, the subsampled curvelet coefficients are calculated directly by restricting the FFT to a bounding box that contains the support of $\hat{c}_j^\alpha[-k]$. A horizontal or vertical warping maps this bounding box to an elongated rectangular frequency box on which the inverse FFT is calculated. One can verify that the resulting coefficients correspond to the subsampled curvelet coefficients. The overall complexity of the algorithm is then $O(N \log_2(N))$, as detailed in [140]. The tight frame redundancy bound obtained with this discrete algorithm is $A \approx 5$.

An orthogonal curvelet type transform has been developed by Do and Vetterli [212]. The resulting contourlets are not redundant but do not have the appropriate time and frequency localization needed to obtain asymptotic approximation results similar to curvelets.

5.6 EXERCISES

5.1 [1] Prove that if $K \in \mathbb{Z} - \{0\}$, then $\{\phi_p[n] = \exp(i2\pi pn/(KN))\}_{0 \leqslant p < KN}$ is a tight frame of $\mathbb{C}^N$. Compute the frame bound.

5.2 [1] Prove that if $K \in \mathbb{R} - \{0\}$, then $\{\phi_p(t) = \exp(i2\pi pnt/K)\}_{p \in \mathbb{Z}}$ is a tight frame of $\mathbf{L}^2[0, 1]$. Compute the frame bound.

5.3 [2] Prove that a finite set of N vectors $\{\phi_n\}_{1 \leqslant n \leqslant N}$ is always a frame of the space **V** generated by linear combinations of these vectors.

5.4 [1] If U_1 and U_2 are two operators from $\mathbb{C}^N$ to $\mathbb{C}^N$, prove that the trace (sum of diagonal values) satisfies $\text{tr}(U_1 U_2) = \text{tr}(U_2 U_1)$.

5.5 [2] Prove that the translation-invariant frame

$$\{\phi_p[n] = \delta[(n-p)\text{mod}N] - \delta[(n-p-1)\text{mod}N]\}_{0 \leqslant p < N}$$

is a translation-invariant frame of the space $\mathbf{V} = \{f \in \mathbb{R}^N : \sum_{n=0}^{N-1} f[n] = 0\}$. Compute the frame bounds. Is it a numerically stable frame when N is large ?

5.6 [2] Construct a Riesz basis in $\mathbb{C}^N$ with a lower frame bound A that tends to zero and an upper frame bound that tends to $+\infty$ as N increases.

5.7 [1] If U is an operator from $\mathbb{C}^N$ to $\mathbb{C}^P$, prove that **Null**U^* is the orthogonal complement of **Im**U in $\mathbb{C}^P$.

5.8 [3] Prove Theorem 5.12.

5.9 [1] Let $\hat{g} = \mathbf{1}_{[-\omega_0, \omega_0]}$. Prove that $\{g(t - p2\pi/\omega_0) \exp(ik\omega_0 t)\}_{(k,p) \in \mathbb{Z}^2}$ is an orthonormal basis of $\mathbf{L}^2(\mathbb{R})$.

5.10 [2] Let $g_{m,k}[n] = g[n - mM] \exp(i2\pi kn/K)$, where $g[n]$ is a window with a support included in $[-K/2, K/2 - 1]$.
  (a) Prove that $\sum_{n=mM-M/2}^{mM+M/2-1} |g[n - mM]|^2 |f[n]|^2 = K^{-1} \sum_{k=0}^{K-1} |\langle f, g_{m,k} \rangle|^2$.
  (b) Prove Theorem 5.18 with arguments similar to Theorem 5.17.

5.11 [2] Compute the trigonometric polynomials $\widehat{\tilde{h}}(\omega)$ and $\widehat{\tilde{g}}(\omega)$ of minimum degree that satisfy (5.63) for the spline filters (5.67, 5.68) with $m = 2$. Compute numerically the graph of $\widehat{\tilde{\phi}}$ and $\tilde{\phi}$. Are they finite-energy functions?

5.12 [1] Compute a cubic spline dyadic wavelet with two vanishing moments using the filter h defined by (5.67) for $m = 3$, with a filter g having three nonzero coefficients. Compute in WAVELAB the dyadic wavelet transform of the Lady signal with this new wavelet. Calculate $\tilde{g}[n]$ if $\tilde{h}[n] = h[n]$.

5.13 [2] Prove the tight-frame energy conservation (4.29) of a discrete windowed Fourier transform. Derive (4.28) from general tight-frame properties. Compute the resulting discrete windowed Fourier transform reproducing kernel.

5.14 [1] Let $\{g(t - n\beta)\exp(ik\eta t)\}_{(n,k)\in\mathbb{Z}^2}$ be a windowed Fourier frame defined by $g(t) = \pi^{-1/4}\exp(-t^2/2)$ with $\beta = \eta$ and $\beta\eta < 2\pi$. With the conjugate gradient algorithm of Theorem 5.8, compute numerically the window $\tilde{g}(t)$ that generates the dual frame, for the values of $\beta\eta$ in Table 5.3. Compare $\tilde{g}$ with g and explain why they are progressively more different as $\beta\eta$ tends to 2π.

5.15 [2] *Sigma–Delta converter.* A signal $f(t)$ is sampled and quantized. We suppose that $\hat{f}$ has a support in $[-\pi/T, \pi/T]$.
(a) Let $x[n] = f(nT/K)$. Show that if $\omega \in [-\pi, \pi]$, then $\hat{x}(\omega) \neq 0$ only if $\omega \in [-\pi/K, \pi/K]$.
(b) Let $\tilde{x}[n] = Q(x[n])$ be the quantized samples. We now consider $x[n]$ as a random vector, and we model the error $x[n] - \tilde{x}[n] = W[n]$ as a white noise process of variance σ^2. Find the filter $h[n]$ that minimizes

$$\varepsilon = E\{\|\tilde{x} \star h - x\|^2\},$$

and compute this minimum as a function of σ^2 and K.
(c) Let $\hat{h}_p(\omega) = (1 - e^{-i\omega})^{-p}$ be the transfer function of a discrete integration of order p. We quantize $\tilde{x}[n] = Q(x \star h_p[n])$. Find the filter $h[n]$ that minimizes $\varepsilon = E\{\|\tilde{x} \star h - x\|^2\}$, and compute this minimum as a function of σ^2, K, and p. For a fixed oversampling factor K, how can we reduce this error?

5.16 [3] *Oversampled analog-to-digital conversion.* Let $\phi_s(t) = s^{1/2}\sin(\pi t/s)/(\pi t)$.
(a) Prove that the following family is a union of orthogonal bases:

$$\left\{\phi_s\left(t - k\frac{s}{K} - ns\right)\right\}_{1 \leq k \leq K, n \in \mathbb{Z}}$$

Compute the tight-frame bound.
(b) Prove that the frame projector P defined in Proposition 5.9 is a discrete convolution. Compute its impulse response $h[n]$.
(c) Characterize the signals $a[n]$ that belong to the image space **ImΦ** of this frame.
(d) Let $f(t)$ be a signal with a Fourier transform supported in $[-\pi/s, \pi/s]$. Prove that $f \star \phi_s(ns) = s^{-1/2}f(ns)$.

(e) Let $s_0 = s/K$. For all $n \in \mathbb{Z}$, we measure the oversampled noisy signal $Y[n] = f \star \phi_s(ns_0) + W[n]$ where $W[n]$ is a Gaussian white noise of variance σ^2. With the frame projector P, compute the error $E\{|PY[Kn] - s^{-1/2}f(ns)|^2\}$ and show that it decreases when K increases.

5.17 [1] Let ψ be a dyadic wavelet that satisfies (5.48). Let $\ell^2(\mathbf{L}^2(\mathbb{R}))$ be the space of sequences $\{g_j(u)\}_{j \in \mathbb{Z}}$ such that $\sum_{j=-\infty}^{+\infty} \|g_j\|^2 < +\infty$.

(a) Verify that if $f \in \mathbf{L}^2(\mathbb{R})$, then $\{Wf(u, 2^j)\}_{j \in \mathbb{Z}} \in \ell^2(\mathbf{L}^2(\mathbb{R}))$. Next, let $\tilde{\psi}$ be defined by

$$\widehat{\tilde{\psi}}(\omega) = \frac{\hat{\psi}(\omega)}{\sum_{j=-\infty}^{+\infty} |\hat{\psi}(2^j \omega)|^2},$$

and W^{-1} be the operator defined by

$$W^{-1}\{g_j(u)\}_{j \in \mathbb{Z}} = \sum_{j=-\infty}^{+\infty} \frac{1}{2^j} g_j \star \tilde{\psi}_{2^j}(t).$$

Prove that W^{-1} is the pseudo inverse of W in $\ell^2(\mathbf{L}^2(\mathbb{R}))$.

(b) Verify that $\tilde{\psi}$ has the same number of vanishing moments as ψ.

(c) Let $\mathbf{V}$ be the subspace of $\ell^2(\mathbf{L}^2(\mathbb{R}))$ that regroups all the dyadic wavelet transforms of functions in $\mathbf{L}^2(\mathbb{R})$. Compute the orthogonal projection of $\{g_j(u)\}_{j \in \mathbb{Z}}$ in $\mathbf{V}$.

5.18 [1] Prove that if there exist $A > 0$ and $B \geqslant 0$ such that

$$A\,(2 - |\hat{h}(\omega)|^2) \leqslant |\hat{g}(\omega)|^2 \leqslant B\,(2 - |\hat{h}(\omega)|^2),$$

and if ϕ defined in (5.59) belongs to $\mathbf{L}^2(\mathbb{R})$, then the wavelet ψ given by (5.60) satisfies the dyadic wavelet condition (5.55).

5.19 [3] *Zak transform.* The Zak transform associates to any $f \in \mathbf{L}^2(\mathbb{R})$

$$Zf(u, \xi) = \sum_{l=-\infty}^{+\infty} e^{i2\pi l \xi} f(u - l).$$

(a) Prove that it is a unitary operator from $\mathbf{L}^2(\mathbb{R})$ to $\mathbf{L}^2[0, 1]^2$:

$$\int_{-\infty}^{+\infty} f(t)\, g^*(t)\, dt = \int_0^1 \int_0^1 Zf(u, \xi)\, Zg^*(u, \xi)\, du\, d\xi,$$

by verifying that for $g = \mathbf{1}_{[0,1]}$, it transforms the orthogonal basis $\{g_{n,k}(t) = g(t - n)\exp(i2\pi kt)\}_{(n,k) \in \mathbb{Z}^2}$ of $\mathbf{L}^2(\mathbb{R})$ into an orthonormal basis of $\mathbf{L}^2[0, 1]^2$.

(b) Prove that the inverse Zak transform is defined by

$$\forall h \in \mathbf{L}^2[0, 1]^2, \quad Z^{-1}h(u) = \int_0^1 h(u, \xi)\, d\xi.$$

(c) Prove that if $g \in \mathbf{L}^2(\mathbb{R})$ then $\{g(t-n) \exp(i2\pi kt)\}_{(n,k)\in\mathbb{Z}^2}$ is a frame of $\mathbf{L}^2(\mathbb{R})$ if and only if there exist $A > 0$ and B such that

$$\forall(u, \xi) \in [0, 1]^2, \quad A \leqslant |Zg(u, \xi)|^2 \leqslant B, \qquad \textbf{(5.117)}$$

where A and B are the frame bounds.

(d) Prove that if (5.117) holds, then the dual window $\tilde{g}$ of the dual frame is defined by $Z\tilde{g}(u, \xi) = 1/Zg^*(u, \xi)$.

5.20 [3] Suppose that $\hat{f}$ has a support in $[-\pi/T, \pi/T]$. Let $\{f(t_n)\}_{n\in\mathbb{Z}}$ be irregular samples that satisfy (5.8). With the conjugate gradient Theorem 5.8, implement numerically a procedure that computes a uniform sampling $\{f(nT)\}_{n\in\mathbb{Z}}$ (from which f can be recovered with the sampling Theorem 3.2). Analyze the convergence rate of the conjugate-gradient algorithm as a function of δ. What happens if the condition (5.8) is not satisfied?

5.21 [2] Prove that if $\psi(x_1, x_2)$ is a directional wavelet having p vanishing moments in a direction $\alpha + \pi/2$ as defined in (5.99), then it is orthogonal to any two-dimensional polynomial of degree $p - 1$.

5.22 [2] Let $\vec{n}_k = (\cos(2k\pi/K), \sin(2k\pi/K)) \in \mathbb{R}^2$.

(a) Prove that $\{\vec{n}_k\}_{0 \leqslant k < K}$ is a tight frame of K vectors and that for any $\omega = (\omega_1, \omega_2) \in \mathbb{R}^2$, it satisfies $\sum_{k=0}^{K-1} |\omega.\vec{n}_k|^2 = K/2|\omega|^2$ where $\omega.\vec{n}$ is the inner product in $\mathbb{R}^2$.

(b) Let $\psi^k = \partial\theta(x)/\partial\vec{n}_k$ be the derivative of $\theta(x)$ in the direction of $\vec{n}_k$ with $x \in \mathbb{R}^2$. If $\theta(x)$ is rotationally invariant (not modified by a rotation of x), then prove that the frame condition (5.101) is equivalent to

$$2A/K \leqslant \sum_{j=-\infty}^{+\infty} 2^{2j} |\omega|^2 |\hat{\theta}(2^j\omega)|^2 \leqslant 2B/K.$$

5.23 [4] Develop a texture classification algorithm with a two-dimensional Gabor wavelet transform using four oriented wavelets. The classification procedure can be based on "feature vectors" that provide local averages of the wavelet transform amplitude at several scales, along these four orientations [315, 338, 402, 467].